Liprin-α2 promotes the presynaptic recruitment and turnover of RIM1/CASK to facilitate synaptic transmission

Samantha A. Spangler,[1] Sabine K. Schmitz,[3] Josta T. Kevenaar,[4] Esther de Graaff,[1,4] Heidi de Wit,[3] Jeroen Demmers,[2] Ruud F. Toonen,[3] and Casper C. Hoogenraad[1,4]

[1]Department of Neuroscience and [2]Proteomics Center, Erasmus Medical Center, 3015GE Rotterdam, Netherlands
[3]Department of Functional Genomics, Center for Neurogenomics and Cognitive Research, VU University Amsterdam, 1081HV Amsterdam, Netherlands
[4]Cell Biology, Faculty of Science, Utrecht University, 3584CH Utrecht, Netherlands

The presynaptic active zone mediates synaptic vesicle exocytosis, and modulation of its molecular composition is important for many types of synaptic plasticity. Here, we identify synaptic scaffold protein liprin-α2 as a key organizer in this process. We show that liprin-α2 levels were regulated by synaptic activity and the ubiquitin–proteasome system. Furthermore, liprin-α2 organized presynaptic ultrastructure and controlled synaptic output by regulating synaptic vesicle pool size. The presence of liprin-α2 at presynaptic sites did not depend on other active zone scaffolding proteins but was critical for recruitment of several components of the release machinery, including RIM1 and CASK. Fluorescence recovery after photobleaching showed that depletion of liprin-α2 resulted in reduced turnover of RIM1 and CASK at presynaptic terminals, suggesting that liprin-α2 promotes dynamic scaffolding for molecular complexes that facilitate synaptic vesicle release. Therefore, liprin-α2 plays an important role in maintaining active zone dynamics to modulate synaptic efficacy in response to changes in network activity.

Introduction

The primary function of the presynaptic active zone (AZ) is to regulate the release of neurotransmitter-filled synaptic vesicles (SVs) in response to action potentials entering the bouton (Südhof, 2012). The SV cycle is tightly controlled, both temporally and spatially, and its performance is modified in response to activity (Atwood and Karunanithi, 2002). Recent experiments show that regulation of presynaptic efficacy involves molecular reorganization of the release apparatus by modulating AZ protein turnover (Lazarevic et al., 2011). Delivery or removal of AZ molecules to or from any given synapse may not only change its release properties but also compromise overall synapse content and dynamics. However, mechanisms of presynapse dynamics are poorly understood and the identity of proteins that function as upstream regulators remains unknown.

Several studies suggest that invertebrate liprin-α family proteins, *Drosophila melanogaster* dliprin-α and *Caenorhabditis elegans* SYD-2, play a key role in presynaptic development (Zhen and Jin, 1999; Kaufmann et al., 2002; Dai et al., 2006; Patel et al., 2006; Astigarraga et al., 2010; Chia et al., 2012; Owald et al., 2012). In addition, liprin-α family proteins in mammals continue to be expressed at high levels in the adult brain and are engaged in high-affinity interactions with many AZ proteins (Spangler and Hoogenraad, 2007). These characteristics make liprin-α an attractive candidate to modulate AZ content and synaptic efficacy. However, because of the complexity of the liprin-α family and its four isoforms, known as liprin-α1, α2, α3, and α4 (Spangler and Hoogenraad, 2007), knowledge of the presynaptic role of liprin-α in mammalian neurons is primarily limited to its expression in mouse brain (Spangler et al., 2011; Zürner et al., 2011), its subcellular localization by electron microscopy (Wyszynski et al., 2002), and its potential binding partners

S.A. Spangler, S.K. Schmitz, and J.T. Kevenaar contributed equally to this paper.

Correspondence to Casper C. Hoogenraad: c.hoogenraad@uu.nl; or Ruud F. Toonen: ruud.toonen@cncr.vu.nl

Abbreviations used in this paper: ANOVA, analysis of variance; AZ, active zone; DIV, day in vitro; EPSC, excitatory postsynaptic current; NB, neurobasal medium; RRP, readily releasable pool; SV, synaptic vesicle; SyPhy, synaptophysinphluorin; TRP, total recycling pool.

The Rockefeller University Press $30.00
J. Cell Biol. Vol. 201 No. 6 915–928
www.jcb.org/cgi/doi/10.1083/jcb.201301011

(Schoch and Gundelfinger, 2006; Spangler and Hoogenraad, 2007). Notably, liprin-α2 expression increases with age, and it is abundant in the adult hippocampus and enriched at mature synapses (Spangler et al., 2011; Zürner et al., 2011). We therefore set out to examine the role of liprin-α2 in mature hippocampal synapses by investigating whether liprin-α2 regulates presynaptic organization by anchoring AZ proteins such as RIM1 and CASK to regulate SV release.

By using biochemical, cell biological, electrophysiological, live-cell imaging, and quantitative microscopy approaches, we show that liprin-α2 organizes presynaptic ultrastructure and controls synaptic output by regulating SV pool size. We propose a model in which liprin-α2 organizes presynaptic composition and controls the dynamics of RIM and CASK in synapses in response to changes in network activity. Our data indicate that liprin-α2 is a unique scaffolding protein that promotes protein dynamics at the AZ and that this local mobility of presynaptic proteins is crucial to support SV release and normal presynaptic output.

Results

Liprin-α2 is regulated by synaptic activity and the ubiquitin–proteasome system

Our previous work indicates that liprin-α2 (Fig. 1 A) is the major liprin-α family member at mature hippocampal presynapses (Spangler et al., 2011). Because it is unknown how liprin-α2 protein levels are regulated at synapses, we examined the turnover of presynaptic liprin-α2. FRAP experiments revealed that GFP–liprin-α2 fluorescence recovers to 67 ± 4% of prebleaching intensity within 8 min with a mean recovery half-time of 13 ± 3 s (Fig. 1, B–D). On this timescale the AZ proteins Munc13 and bassoon exhibit very little recovery (Kalla et al., 2006; Tsuriel et al., 2009), indicating that liprin-α2 is a relatively dynamic component of the presynaptic AZ. Because the ubiquitin–proteasome system plays an important role in synaptic protein turnover (Tai and Schuman, 2008; Bingol and Sheng, 2011), we tested whether the proteasome inhibitor MG132 affects liprin-α2 expression in hippocampal neurons. Brief application of MG132 (10 µM, 1 h) caused an increase in synaptic liprin-α2, in contrast to synaptic markers PSD-95 or bassoon (Fig. 1, E and F). In addition, FRAP experiments showed that application of MG132 (10 µM, 4 h) results in an increase in the turnover of presynaptic liprin-α2 (82 ± 5%, $t_{1/2}$ = 22 ± 4 s; Fig. 1, B–D), indicating that mammalian liprin-α2 is regulated by proteasomal degradation. We next examined whether changes in global synaptic network activity can also affect liprin-α2 levels. Decreasing network activity for 48 h via the voltage-gated Na^+ channel blocker TTX (2 µM) or the NMDA-receptor antagonist APV (50 µM) and AMPA receptor antagonist DNQX (10 µM) led to a significant decrease in liprin-α2 levels, whereas application of the $GABA_A$ receptor antagonist Bicuculline (40 µM, 48 h) to increase network activity showed an ∼30% increase in liprin-α2 levels (Fig. 1 G). Consistently, comparable results were obtained when we measured total liprin-α2 levels using Western blotting. Application of TTX or APV/DNQX resulted in an ∼70% and ∼55% reduction of liprin-α2 levels compared with control, respectively (Fig. 1, H and I). Furthermore, MG132 (10 µM, 6 h) increased global liprin-α2 levels in addition to partially occluding the loss of liprin-α2 caused by TTX (Fig. 1, H and I). The same trend is observed for the combined MG132 and APV/DNQX treatments; however, the difference was not statistically significant. These data indicate that liprin-α2 is a dynamic member of the presynaptic AZ; its levels scale with network activity, and proteasome-mediated degradation both maintains steady-state levels of liprin-α2 and contributes substantially to TTX-induced loss of liprin-α2.

Liprin-α2 regulates SV release

Next, we examined whether liprin-α2 affects presynaptic function through acute depletion of liprin-α2 expression in mature hippocampal presynapses. We selected two independent liprin-α2 shRNAs and one control liprin-α1 shRNA, all of which were effective in reducing protein levels of the targeted isoform without affecting the expression of other liprin-α proteins (Fig. 2, A–F; and Table S1). We first investigated the effect of liprin-α2 knockdown on SV recycling using fluorescent membrane FM dyes (Fernández-Alfonso and Ryan, 2004). At day in vitro (DIV) 19, we labeled the total recycling pool (TRP) of vesicles of hippocampal neuron cultures that were transfected at DIV15 with liprin-α2 shRNA by stimulation with 70 mM KCl for 90 s in the presence of 10 µM FM4-64 dye (Leal-Ortiz et al., 2008) and analyzed the extent of FM dye loading and unloading in transfected axons that formed synapses with untransfected postsynaptic neurons. There were no significant differences in the percentage of axonal varicosities that contained FM4-64 clusters, indicating that liprin-α2 does not influence the number of active synapses (Fig. 2 G). However, after loading, synapses deficient in liprin-α2 displayed an ∼17% reduction of FM4-64 fluorescence intensity compared with control (Fig. 2 H). We further compared the destaining kinetics of the TRP after a second stimulation with 70 mM KCl for 60 s. Neurons expressing liprin-α2 shRNA exhibited decreased FM4-64 unloading both in the frame immediately after stimulation and in the two minutes that followed (Fig. 2, I and J). This suggests that liprin-α2 controls TRP size and regulates the efficiency of SV release.

Liprin-α2 regulates readily releasable pool (RRP) size and synaptic plasticity

To understand the presynaptic function of liprin-α2 in greater detail, we performed whole-cell patch clamp recordings in cultured hippocampal autaptic neurons. Neurons were infected with liprin-α2 shRNA expressing lentiviruses at DIV9, after synapses are formed in this system (Gekel and Neher, 2008; Weston et al., 2011), and analyzed at DIV14. Spontaneous release characteristics such as miniature excitatory postsynaptic current (EPSC) amplitude (Fig. 3, A and B), frequency (Fig. 3 C), rise time (Fig. 3 D), and charge (Fig. 3 E) were unchanged. Hence, deletion of liprin-α2 does not affect postsynaptic receptor sensitivity and vesicle filling, nor does it interfere with the neuron's capacity to spontaneously release SVs. However, evoked response amplitudes (EPSC amplitudes) were decreased by >40% in neurons lacking liprin-α2 (Fig. 3 F). A second independent shRNA against liprin-α2 showed a similar phenotype (Fig. S1 A), whereas liprin-α1 knockdown and a scrambled shRNA did not

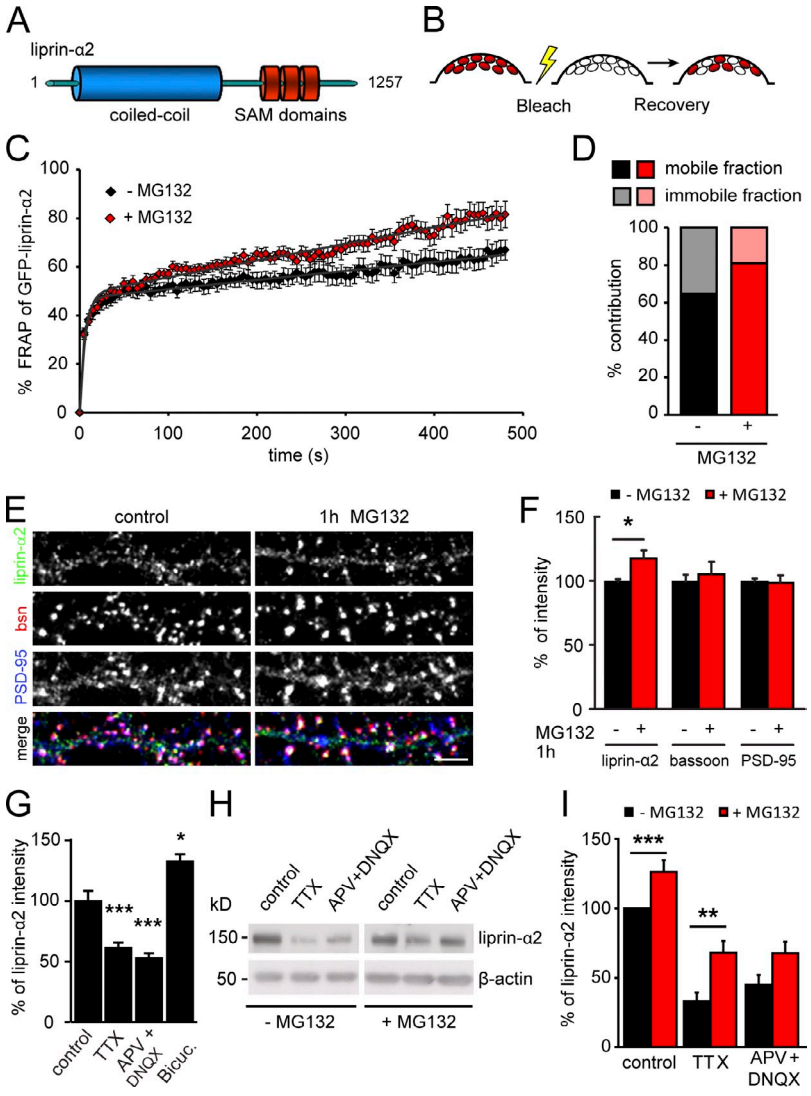

Figure 1. **Liprin-α2 is regulated by synaptic activity and the ubiquitin–proteasome system.** (A) Domain structure of liprin-α2. (B) Schematic representation of FRAP procedure. Fluorescent-tagged proteins (red ovals) are bleached (white ovals) and fluorescence recovery is monitored in a single synapse. (C) Mean recovery time course of GFP-liprin-α2 treated with 10 µM of the proteasome inhibitor MG132 or DMSO as a control for 4 h in DIV15+4 neurons. Data were fit according to a two-exponential model (dark gray lines). ANOVA repeated measures: n = 32/32, F = 5.04, P = 0.028. n = 2 independent experiments. (D) Quantification of the mobile and immobile fractions of GFP-liprin-α2 treated with 10 µM MG132 or DMSO for 4 h in DIV15+4 neurons according to the fitted recovery time course (DMSO: mobile, 65%; immobile, 35%; MG132: mobile, 82%; immobile, 18%). (E) Representative images of endogenous liprin-α2 (green), bassoon (red), and PSD-95 (blue) in DIV19 hippocampal neurons treated with 10 µM of the proteasome inhibitor MG132 for 1 h before fixation. Bar, 5 µm. (F) Quantification of endogenous synaptic liprin-α2, bassoon, and PSD-95 levels in cells treated with 10 µM MG132 for 1 h. n = 5; *, P = 0.02. (G) Quantification of endogenous somatic liprin-α2 levels in DIV21 neurons treated with 2 µM TTX, 50 µM APV and 10 µM DNQX, 40 µM Bicuculline, or DMSO (control) for 48 h. n = 7/10; ***, P < 0.0005; *, P = 0.011. (H) Western blots of extracts of DIV14 hippocampal neuron cultures treated with 2 µM TTX, 50 µM APV, and 10 µM DNQX or DMSO (control) for 48 h with or without 10 µM MG132 treatment for 6 h. Equal volumes of extracts were loaded and immunoblotted for liprin-α2 and β-actin as loading control. (I) Quantification of endogenous liprin-α2 levels in cells treated with TTX, APV, and DNQX or DMSO (control) for 48 h with or without MG132 for 6 h. n = 8/14; ***, P < 0.001; **, P = 0.003; n = 4 independent experiments. Data are presented as mean values ± SEM.

affect synaptic responses (Fig. S1, B–F). Importantly, overexpression of a shRNA-resistant liprin-α2 largely rescued the knockdown phenotype (Fig. S1 G).

We next investigated the RRP size in liprin-α2 knockdown cells by measuring responses to application of 500 mM sucrose (Rosenmund and Stevens, 1996). Liprin-α2–deficient neurons showed an ∼60% decrease in RRP size (Fig. 3 G), whereas the vesicular release probability (P_{ves}) was unchanged (Fig. 3 H). Therefore, in addition to regulating the TRP, liprin-α2 is an important factor in determining the number of vesicles present in the RRP. Furthermore, cells were stimulated with paired pulses of varying interstimulus intervals to test the effect of liprin-α2 deletion on short-term changes in synaptic strength. Neurons expressing liprin-α2 shRNA exhibited paired pulse facilitation (Fig. 3 I), indicating that synaptic release probability is decreased in the absence of liprin-α2. In all electrophysiological parameters, no significant differences were observed in neurons expressing control shRNAs (Fig. S1), further confirming that liprin-α2 is specifically important for normal presynaptic function in the hippocampus.

To fully rule out any contribution of postsynaptic effects on the presynaptic phenotype, as well as determine if liprin-α2 deficiency affects all synapses equally, we probed SV release in presynapses with untransfected postsynaptic partners using the optical reporter synaptophysinphluorin (SyPhy; Granseth et al., 2006). Neurons were transfected with SyPhy plus liprin-α2 shRNA or scrambled shRNA as control at DIV10 and imaged 5 d later. SV release was triggered by applying 200 AP stimuli at 20 Hz and Syphy responses were measured across 15–30 boutons per individual neuron. Signals were normalized to the maximal fluorescence obtained at each bouton upon NH_4Cl superfusion to instantly alkalize the entire labeled vesicle pool (Fig. 3 J). Expression of liprin-α2 shRNA strongly diminished SV exocytosis upon stimulation (Fig. 3 K) and the mean maximal amplitude was more than fourfold reduced compared with scrambled controls (Fig. 3 L, scrambled [WT], 0.22 ± 0.05, n = 8; α2 KD, 0.05 ± 0.03, n = 6; 15–30 synapses per cell; **, P = 0.012). Examination of exocytosis at individual boutons revealed that liprin-α2 reduction resulted in an overall reduction of release probability and increased the number of presynaptically silent synapses. Together, the combination of probing exocytosis in mass cultures using FM-dye and SyPhy measurements and using patch clamp physiology in autaptic cultures reveals

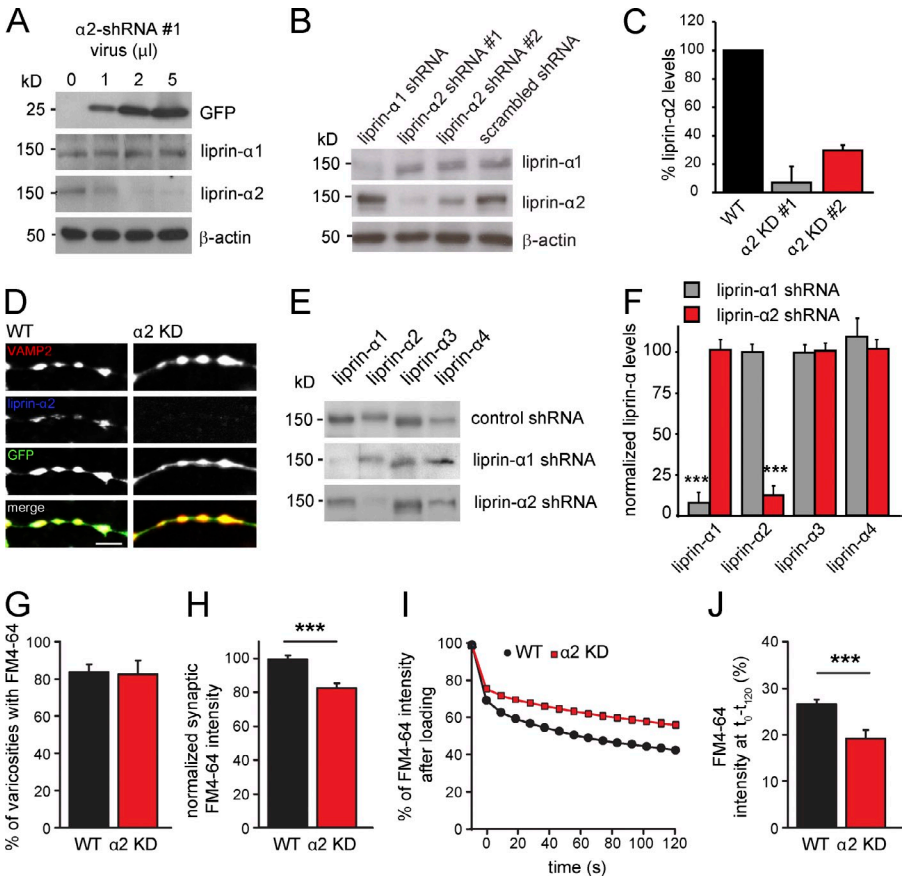

Figure 2. **Liprin-α2 regulates SV release.** (A) Western blots of extracts of DIV13 hippocampal neuron culture infected at DIV7 with indicated amount of liprin-α2 shRNA expressing lentivirus. Equal volumes of extracts were loaded and immunoblotted for GFP, liprin-α1, liprin-α2, and actin as a loading control. (B) Western blots of extracts of DIV13 neurons infected at DIV7 with liprin-α1 shRNA, liprin-α2 shRNA #1, liprin-α2 shRNA #2, or scrambled shRNA lentivirus as control. Equal volumes of extract were loaded and immunoblotted for liprin-α1, liprin-α2, and actin as a loading control. (C) Quantification of knockdown of endogenous liprin-α2 with liprin-α2 shRNA. For Western blot, DIV7 neurons were infected with indicated liprin-α2 shRNA constructs and harvested 6 d later. (D) Representative images of liprin-α2 levels in neurites of neurons infected either with GFP or liprin-α2 shRNA lentivirus (green). Cells were stained for endogenous VAMP2 (red) and liprin-α2 (blue). Bar, 5 µm. (E) Western blots of GFP expression in extracts of HeLa cells cotransfected with GFP-liprin-α1, -α2, -α3, or- α4 and either liprin-α1, liprin-α2, or control (CASK) shRNA constructs. (F) Quantification of knockdown of GFP-liprin-α protein with liprin-α1, liprin-α2, or control (CASK) shRNA constructs, normalized to control. $n = 3$; ***, $P = 0.0001$. (G) Quantification of the percentage of presynaptic sites transfected with liprin shRNA constructs that were loaded with FM4-64 dye (GFP: 84.0 ± 4.3%; liprin-α2 shRNA: 83.0 ± 7.3%; $n = 5$ sets of 20 synapses per group). (H) Quantification of the fluorescence intensity of FM4-64 dye loading of presynaptic sites transfected with liprin shRNA constructs (GFP: 100.0 ± 2.3%; liprin-α2 shRNA: 83.2 ± 2.9%; $n = 100$ synapses per group; ***, $P < 0.0005$). Intensity of FM4-64 labeling in control cells was set to 100%. (I) Quantification FM4-64 destaining after unloading of presynapses transfected with liprin shRNA constructs ($n = 75$ [GFP] or 82 [liprin-α2 shRNA] synapses; for GFP vs. liprin-α2 shRNA ANOVA repeated measures: ***, $P < 0.0005$, $F = 51.96$). (J) Quantification of the difference between the first frame after unloading stimulation (t_0) and the last frame imaged (t_{120}) for presynapses transfected with liprin shRNA constructs (GFP: 26.8 ± 1.0 AU, $n = 75$ synapses; liprin-α2 shRNA: 19.4 ± 1.9 AU, $n = 82$ synapses; ***, $P = 0.0005$). Data are presented as mean values ± SEM.

that liprin-α2 is an essential component of the presynaptic machinery that orchestrates activity-dependent SV release.

Liprin-α2 organizes presynaptic ultrastructure

Acute liprin-α2 knockdown did not affect neuronal morphology or synapse density, as soma area, dendrite length, and branching as well as synapse number were similar to control neurons (Fig. 4, A–F). Synapse density (Fig. 4 B) was not significantly different in liprin-α2–deficient neurons, though, consistent with earlier observations in *C. elegans* SYD-2 mutants (Zhen and Jin, 1999), synapses were slightly elongated in the absence of liprin-α2 (Fig. 4, G–I). Close examination of synaptic ultrastructure using electron microscopy (Fig. 5 A) confirmed many of our electrophysiological and immunocytochemical findings. Consistent with the observed decrease in RRP size (Fig. 3 G), docked vesicles were reduced with liprin-α2 knockdown (Fig. 5 B). Furthermore, as expected because of the lengthening of synapses in absence of liprin-α2, liprin-α2 knockdown increases the perimeter of the SV cluster (Fig. 5 C), whereas the total number of SVs was unchanged (Fig. 5 D). Intriguingly, synapses lacking liprin-α2 show a reduced number of vesicles per micrometer perimeter (Fig. 5 E) as well as shortened AZ and postsynaptic density length (Fig. 5, F and G). Hence, these data show that liprin-α2 controls synaptic ultrastructure in mature synapses and implies that liprin-α2 regulates presynaptic function by organizing SVs and the clustering of the presynaptic release machinery.

Liprin-α2 organizes presynaptic protein composition

To investigate the molecular mechanism by which liprin-α2 influences presynaptic function, we first identified liprin-α2 binding partners in the brain using pull-down assays combined with mass spectrometry (Table S2). We identified multiple presynaptic targets, notably the AZ proteins RIM1 and CASK, which have previously been shown to interact with liprin-α family proteins and play important roles in presynaptic function (Schoch et al., 2002). To test where liprin-α2 functions in this presynaptic protein network, we examined synaptic targeting of liprin-α2 after depleting the expression of the liprin-α2 interacting proteins RIM1 and CASK and other prominent AZ proteins, including ELKS1 and 2, bassoon, and piccolo, in cultured hippocampal neurons. Neurons were transfected at DIV15 with shRNA constructs and synaptic expression levels were examined 4 d later (for experimental details, see Fig. S2, Table S1, and Materials and methods). The shRNAs effectively reduced synaptic expression

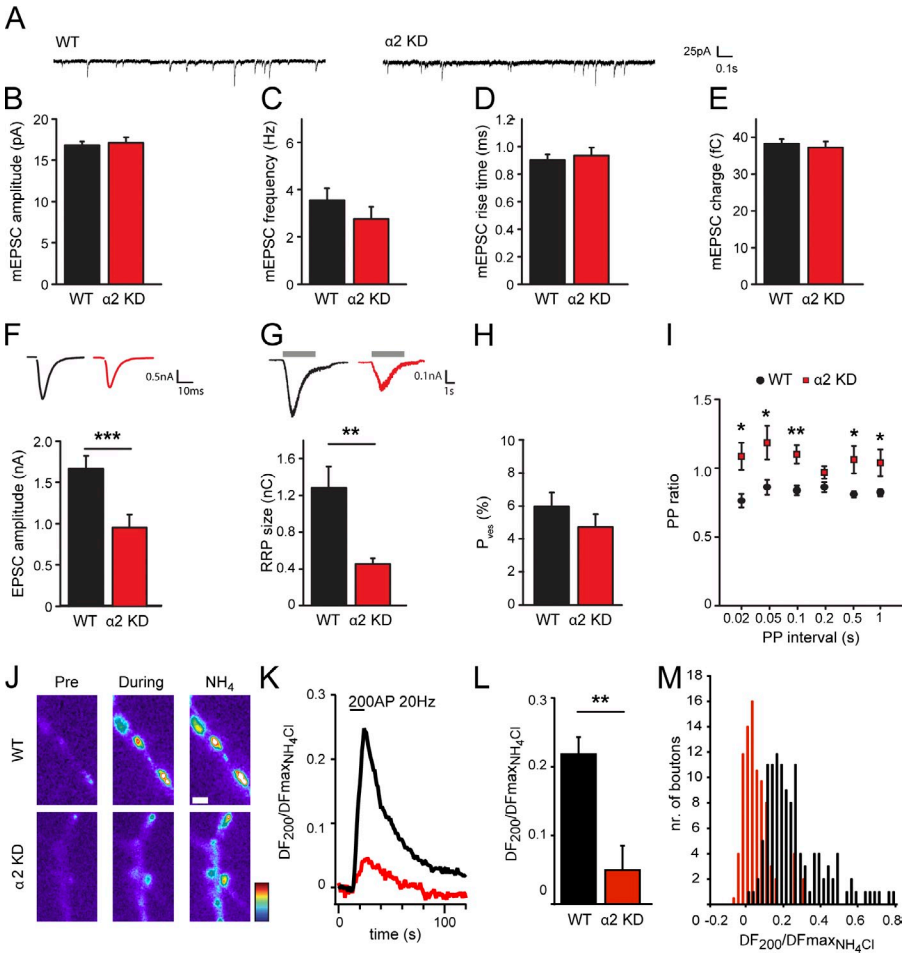

Figure 3. **liprin-α2 regulates RRP size and synaptic plasticity.** (A) Typical examples of spontaneous vesicle release. (B) Amplitude of spontaneous release events in hippocampal autapses infected with liprin shRNA viruses (GFP: 16.9 ± 0.4 pA, *n* = 58; liprin-α2 shRNA: 17.2 ± 0.6, *n* = 37). (C) Spontaneous release frequency in hippocampal autapses infected with liprin shRNA viruses (GFP: 3.6 ± 0.5 Hz, *n* = 60; liprin-α2 shRNA: 2.8 ± 0.5 Hz, *n* = 40;). (D) Rise time of spontaneous release events in hippocampal autapses infected with liprin shRNA viruses (GFP: 0.91 ± 0.04 ms, *n* = 58; liprin-α2 shRNA: 0.94 ± 0.06 ms, *n* = 37). (E) Charge of spontaneous release events in hippocampal autapses infected with liprin shRNA viruses (GFP: 38.4 ± 1.2 fC, *n* = 58; liprin-α2 shRNA: 37.4 ± 1.6 fC, *n* = 37). (F) Amplitude of excitatory synaptic response evoked by an action potential in hippocampal autapses infected with liprin shRNA viruses (GFP: 1.67 ± 0.15 nA, *n* = 73; liprin-α2 shRNA: 0.96 ± 0.16 nA, *n* = 39; ***, P < 0.001). Insets show typical individual traces of EPSCs. Fig. S1 shows a similar reduction of EPSC amplitude using a second independent liprin-α2 shRNA. (G) RRP size as assessed with single hyperosmotic sucrose application (500 mM sucrose) in hippocampal autapses infected with liprin shRNA viruses (GFP: 1.29 ± 0.23 nC, *n* = 19; liprin-α2 KD, 0.46 ± 0.06 nC, *n* = 16; **, P = 0.006). Insets show typical examples of sucrose-induced currents. Gray bars represent time of sucrose application. (H) Vesicular release probability (P_{ves}) is calculated as EPSC charge divided by sucrose-induced RRP charge (GFP: 6.0 ± 0.8%, *n* = 19; liprin-α2 KD, 4.8 ± 0.8, *n* = 16; NS, P = 0.058). (I) Paired-pulse ratio (ratio of the second to the first synaptic response plotted as a function of the stimulus interval) in hippocampal autaptic neurons infected with liprin shRNA viruses. *n* = 37 (GFP) or 21 (liprin-α2 shRNA); PP (20 ms): *, P = 0.012; PP (50 ms): *, P = 0.018; PP (100 ms): **, P = 0.002; PP (200 ms): NS, P = 0.085; PP (500 ms): *, P = 0.044; PP (1,000 ms): *, P = 0.044. (J) Pseudocolored images of the fluorescent response before (Pre) and during 200 AP stimulation and upon NH_4Cl superfusion to probe the total vesicle pool in hippocampal mass cultures transfected with SyPhy plus scrambled shRNA or liprin-α2 shRNA. Bar, 1 µm. (K) Mean fluorescence responses upon 200 AP at 200 Hz in neurons expressing SyPhy plus scrambled shRNA (black trace, *n* = 8 cells) or liprin-α2 shRNA (red trace, *n* = 6 cells) normalized to the maximal NH_4Cl response. 15–30 synapses per cell. (L) Mean values of amplitudes of 200 AP at 20 Hz responses in neurons expressing SyPhy plus scrambled shRNA (WT) or liprin-α2 shRNA (α2 KD) normalized to the maximal NH_4Cl response. WT: 0.22 ± 0.05, *n* = 8; α2 KD: 0.05 ± 0.03, *n* = 6; 15–30 synapses per cell; **, P = 0.012). (M) Distribution of amplitudes in single boutons from neurons expressing SyPhy plus scrambled shRNA (black bars, *n* = 8 cells) or liprin-α2 shRNA (red bars, *n* = 6 cells) normalized to the maximal NH_4Cl response. 15–30 synapses per cell. Data are presented as mean values ± SEM.

levels of the respective proteins (Fig. 6 A). However, under all conditions, no significant change in liprin-α2 clustering at synapses was observed, including when both bassoon and piccolo were simultaneously depleted (Fig. 6, B and C). Thus, synaptic targeting of liprin-α2 in mature axons is not dependent on the presence of other major presynaptic scaffolding proteins.

Next, we examined whether acute depletion of liprin-α2 in mature neurons affects synaptic recruitment of other AZ proteins. Interestingly, we observed an ∼35% decrease in synaptic levels of both CASK (Fig. 6, D and E) and RIM1/2 (Fig. 6, D and F) upon liprin-α2 knockdown. PSD-95 and Shank levels in apposed, untransfected postsynapses were unaffected (Fig. 6, G and H), indicating that postsynaptic organization remained intact in spite of the presynaptic defects. Furthermore, in hippocampal neurons infected with liprin-α2 shRNA expressing lentiviruses we found partial depletion of additional presynaptic proteins, such as AZ components bassoon and Munc18-1, SV proteins Rab3, VAMP2 and synapsin, the vesicular glutamate transporter vGlut, and P/Q type voltage-gated Ca^{2+} channels (Cav2.1), in synapses (Fig. 6, I and J). Next, we tested whether overexpression of the direct binding partners of liprin-α2, RIM1 and CASK, could rescue the liprin-α2 knockdown phenotype. Though lentiviral-mediated expression of both RIM1 and CASK resulted in increased amounts of these proteins at synapses (Fig. 7 A), neither was able to rescue EPSC amplitudes in liprin-α2–deficient neurons (Fig. 7 B). This suggests that liprin-α2 is a critical player in the organization of the presynapse and functions upstream of its direct binding partners RIM and CASK.

Liprin-α2 is important for RIM1 and CASK dynamics at presynapses

To further understand the molecular mechanism by which liprin-α2 regulates RIM1 and CASK at synapses, we tested whether liprin-α2 controls the extent to which they are regulated by activity (Lazarevic et al., 2011). Surprisingly, liprin-α2 does not influence total cellular levels of RIM and CASK and is

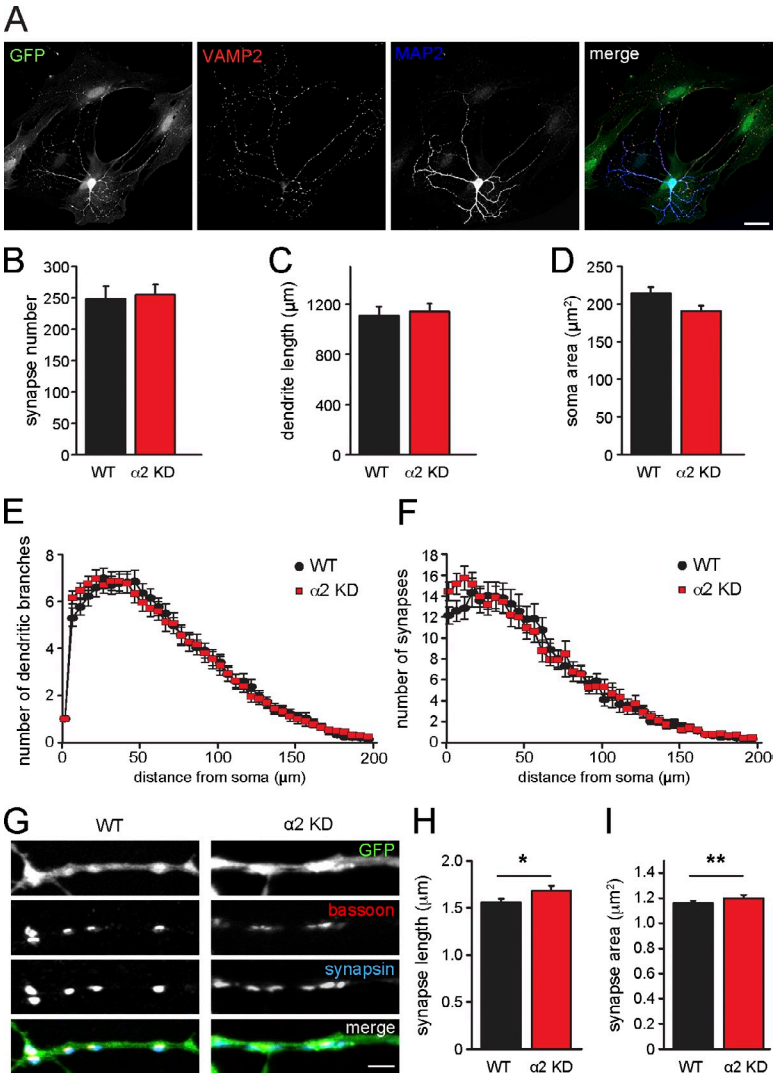

Figure 4. **Liprin-α2 knockdown causes lengthening of presynapses.** (A) Representative images of a hippocampal autaptic neuron expressing GFP stained for MAP2 (blue) and VAMP2 (red) at DIV14. Bar, 30 µm. (B) Quantification of total synapse number in hippocampal autapses infected with GFP or GFP plus liprin-α2 shRNA viruses. n = 70/70. (C) Quantification of total dendrite length in hippocampal autapses infected with GFP or GFP plus liprin-α2 shRNA viruses. (D) Quantification of soma area in hippocampal autapses infected with liprin-α2 shRNA viruses. (E) Quantification of dendritic branching by Sholl analysis in hippocampal autapses infected with control (black line) and liprin-α2 (red line) shRNA viruses. (F) Quantification of number of synapses per distance from the soma (using concentric rings of Sholl analysis) in hippocampal autapses infected with control (black line) and liprin-α2 (red line) shRNA viruses. (G) Representative image of hippocampal autaptic neurons infected with GFP or GFP plus liprin-α2 shRNA stained for bassoon (red) and synapsin (blue). Bar, 5 µm. (H) Quantification of presynapse length in neurons transfected with mCherry and GFP or GFP plus liprin-α2 shRNA. n = 87/90; *, P = 0.04. (I) Quantification of presynapse area in hippocampal autaptic neurons infected with liprin-α2 shRNA. n = 189/211 cells; **, P = 0.007. Data are presented as mean values ± SEM.

not involved in the activity-dependent regulation of total cellular RIM and CASK levels (Fig. 7 C). This implies that liprin-α2's influence on RIM and CASK occurs much more locally and dynamically. Accordingly, we examined the effect of liprin-α2 depletion on the dynamics of these proteins in synapses using FRAP. In wild-type synapses, both RIM1 and CASK (Fig. 8, A–E) showed even more rapid recovery than liprin-α2 (Fig. 1, C and D). Cherry-RIM1 fluorescence recovered to 78 ± 5% of prebleaching intensity within 5 min with a mean recovery $t_{1/2}$ of 17 ± 5 s and remained stable for up to 15 min (Fig. 8, A, C, and E). Cherry-CASK exhibited slightly higher fluorescence recovery (87 ± 6%, $t_{1/2}$ = 7 ± 1 s; Fig. 8, B, D, and E). Because RIM1 and CASK bind directly to liprin-α2, we expected that reduction of liprin-α2 would promote RIM1 and CASK dynamics at synapses and thus increase fluorescent recovery levels in FRAP experiments. Interestingly, liprin-α2 depletion in fact resulted in a significant reduction of presynaptic RIM1 and CASK recovery (Fig. 8 A, RIM1: 60 ± 6%, $t_{1/2}$ = 10 ± 2 s; Fig. 8, B and D, CASK: 70 ± 5%, $t_{1/2}$ = 10 ± 2 s). Hence, although absence of liprin-α2 leads to a reduction in synaptic levels of RIM1 and CASK (Fig. 6, D–F), the remaining RIM1 and CASK molecules appear to be more stable (Fig. 8 E). Finally, to test the mobility of RIM1 and CASK proteins that arrived during the recovery phase and exclude potential FRAP artifacts arising from photoinduced immobile fractions (Lippincott-Schwartz et al., 2003), we performed a second FRAP experiment at the same synapses after 5.5 min (Fig. 8 F). As expected, cherry-CASK and cherry-RIM1 fluorescence recovered to ∼100% of the second prebleach intensity (Fig. 8, F–H), arguing that these results are not caused by photodamage and suggesting that the newly arrived RIM1 and CASK proteins are not yet in a stable complex with liprin-α2 in the synapse. Together, these data indicate that liprin-α2 regulates both the amount and mobility of RIM and CASK at presynaptic terminals.

Discussion

In this study we show that liprin-α2 is an important regulator of presynaptic function and dynamics in mature hippocampal synapses. Its expression levels are controlled by the ubiquitin proteasome system and positively scale with network activity. Liprin-α2 organizes presynaptic ultrastructure and controls synaptic output by regulating SV pool size. We propose a model in which the dynamic recruitment of major AZ constituents like

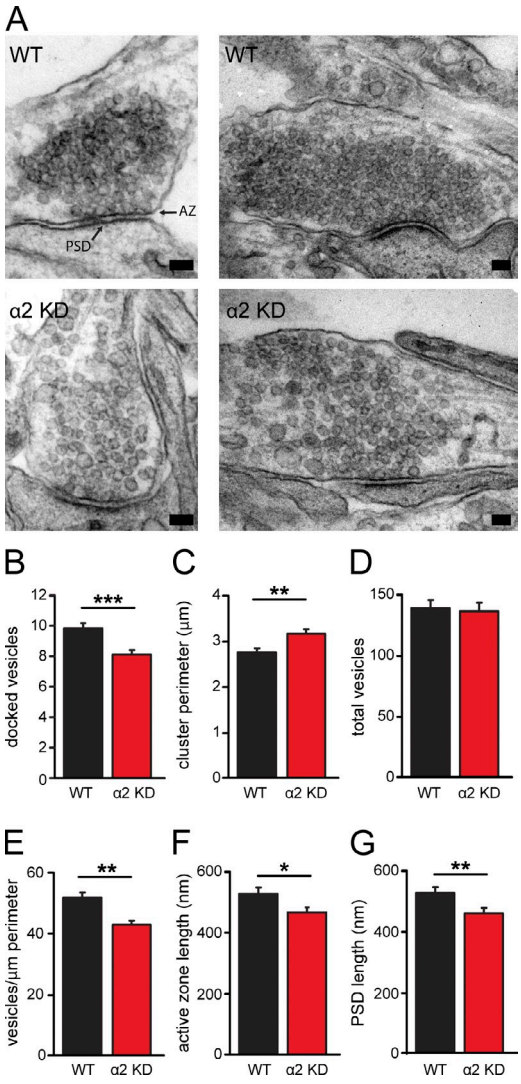

Figure 5. **Liprin-α2 knockdown changes synapse ultrastructure.** Electron microscopy analysis of rat hippocampal autaptic neurons mice infected with lentiviruses expressing GFP or Liprin-α2 shRNA together with GFP. *n* = 3 cultures; GFP: *n* = 150 synapses; α2 KD: *n* = 135 synapses. Graphs represent synapse averages. All data are expressed as mean ± SEM. Mann-Whitney test: *, P < 0.05; **, P < 0.005; ***, P < 0.001. Typical examples are shown in A. Bar, 100 nm. Quantifications are shown in B–G.

RIM1 and CASK by liprin-α2 provides the plasticity needed by the presynaptic terminal to respond to changes in network activity. These data provide surprising new insight into the way presynaptic signaling is controlled and indicate that proper maintenance of presynapse function is dependent on regulating protein dynamics as well as AZ content.

Liprin-α2 levels are strongly regulated by activity

Liprin-α2 is particularly susceptible to activity-dependent regulation and scales with network activity in a nonhomeostatic manner: low activity reduces liprin-α2 levels, whereas increasing activity results in more liprin-α2. Hence, liprin-α2 expression levels respond to network activity to ensure optimal presynaptic output. The suppression of liprin-α2 levels upon blocking neuronal activity depends at least partially on the ubiquitin–proteasome system (Fig. 1). Earlier studies demonstrated regulation of liprin-α family proteins by neuronal activity and the E3 ubiquitin ligase anaphase promoting complex in *D. melanogaster* (van Roessel et al., 2004) and mammalian neurons (Hoogenraad et al., 2007; Lazarevic et al., 2011) and showed that this had important consequences for controlling neuromuscular junction size and dendrite outgrowth, as well as implicated liprin-α as a potential master target for presynaptic anaphase promoting complex (van Roessel et al., 2004; Hoogenraad et al., 2007; Lazarevic et al., 2011). Our data confirms that this regulation is conserved for liprin-α2 at mammalian presynapses and highlights that proteasomal modulation of presynaptic liprin-α2 extends beyond controlling total liprin levels into controlling local liprin-α2 dynamics.

Liprin-α2 controls synaptic output

The liprin-α family has previously been well characterized as a regulator of presynaptic development, particularly in invertebrate model systems. Mutations in *syd-2*, the *C. elegans* homologue of mammalian liprin-α, results in presynapses with a lengthened AZ and insufficient SV clustering (Zhen and Jin, 1999), and SYD-2 is critical for the recruitment of many AZ proteins in a hierarchical manner (Dai et al., 2006; Patel et al., 2006). Additionally, *D. melanogaster dliprin-α* is important in axon guidance (Choe et al., 2006; Hofmeyer et al., 2006), synapse formation (Kaufmann et al., 2002; Astigarraga et al., 2010), and SV trafficking (Miller et al., 2005). These studies, combined with the high degree of evolutionary conservation of the liprin-α family (Spangler and Hoogenraad, 2007), suggest that liprin-α is also likely to be critical in vertebrate neurodevelopment. However, the extent to which liprin-α influences neurons after development is poorly understood.

By using acute knockdowns in cultured neurons after synapse formation, we showed that liprin-α2 levels control the TRP (Fig. 2) and RRP sizes as well as short-term changes in presynaptic strength (Fig. 3). The results from the different vesicle release paradigms imply that liprin-α2 reduction causes reduced synaptic release probability caused by smaller vesicle pool sizes without affecting the release probability of individual SVs. This phenotype strongly resembles that of RIM1 null mutant neurons (Calakos et al., 2004). The decreased AZ length and number of docked SVs in liprin-α2 knockdown neurons (Fig. 5) correlate with the changes in presynaptic strength and are consistent with the reported relationship between AZ length and SV pool size (Schikorski and Stevens, 1997, 1999). Moreover, activity-dependent changes in AZ size have also been shown to relate to changes in SV RRP sizes (Matz et al., 2010). Notably, gross neuronal morphology and total size of the nonrecycling SV pool are unchanged upon loss of liprin-α2, further indicating that, in mature synapses, liprin-α2 primarily influences localized factors within the AZ itself.

Importantly, previous studies in cultured neurons have demonstrated effects of liprin-α on AMPA receptor trafficking (Wyszynski et al., 2002; Ko et al., 2003; Dunah et al., 2005) and dendrite morphology (Dunah et al., 2005; Hoogenraad et al., 2007). These studies used dominant-negative proteins that inhibited

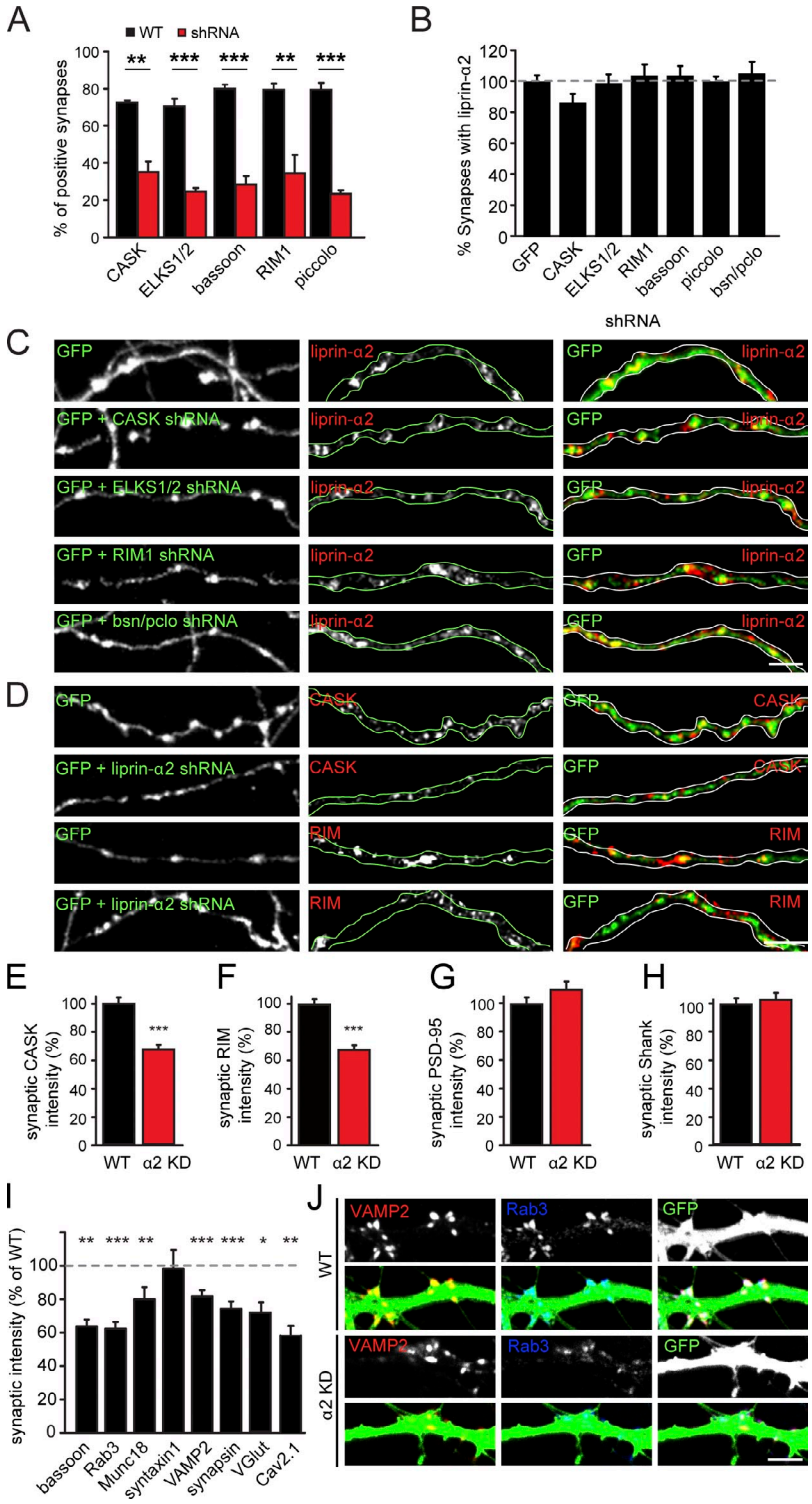

Figure 6. **Liprin-α2 controls presynaptic protein levels.** (A) Quantification of shRNA knockdown of CASK, ELKS1/2, RIM1, bassoon, and piccolo at synapses. *n* = 5–7; 20 synapses/cell. **, P < 0.001; ***, P < 0.0001. (B) Quantification of endogenous liprin-α2 clustering at presynaptic sites transfected at DIV15 with shRNAs of presynaptic proteins and fixed after 4 d. *n* = 5; 20 synapses/cell. (C) Representative images of cells transfected with indicated shRNA and imaged for GFP (green) and endogenous liprin-α2 (red). Bar, 5 µm. (D) Representative images of cells transfected with GFP or GFP plus liprin-α2 shRNA and imaged for GFP (green) and endogenous CASK or RIM1/2 (red). Bar, 5 µm. (E–H) Quantification of fluorescence intensity of endogenous CASK (E) and RIM1/2 (F) at presynaptic sites and PSD-95 (G) and shank (H) at postsynaptic sites transfected with GFP or GFP plus liprin-α2 shRNA at DIV15 and fixed 4 d later. Intensity of synaptic labeling in control cells was set to 100%. *n* = 100 synapses; ***, P < 0.0005. (I) Quantification of fluorescence intensity of various synaptic proteins at presynaptic sites in autaptic neurons infected with GFP or GFP plus liprin-α2 shRNA expressing lentiviruses at DIV9 and fixed 4 d later. Intensity in GFP cells was set to 100%. *n* = 18–49 cells; *, P < 0.05; **, P < 0.005; ***, P < 0.001. (J) Representative images of synaptic Rab3 levels in neurons infected with GFP or liprin-α2 shRNA lentivirus (green). Cells were stained for endogenous VAMP2 (red) and Rab3 (blue). Bar, 5 µm. Data are presented as mean values ± SEM.

interactions of all liprin-α family members with AMPA receptor binding proteins. In this study, using specific liprin-α2 shRNAs, we did not find any evidence for a postsynaptic role of liprin-α2. Spontaneous release amplitudes were normal in autaptic liprin-α2–deficient neurons and presynaptic release was strongly affected in liprin-α2–deficient neurons that made synapses onto wild-type postsynaptic neurons in our imaging paradigms using FM dyes or SyPhy to probe vesicle release. Though we cannot formally rule out that depletion of liprin-α2 would be detrimental to expressing plasticity phenomena involving postsynaptic changes (like, for instance, long-term potentiation), the fact that miniature EPSC characteristics are normal in liprin-α2–deficient neurons and the presence of notable SV release defects in presynapses with wild-type postsynapses strongly support the conclusion that liprin-α2, like its invertebrate homologues SYD-2 and dliprin-α, is most critical for regulating presynaptic properties in hippocampal neurons.

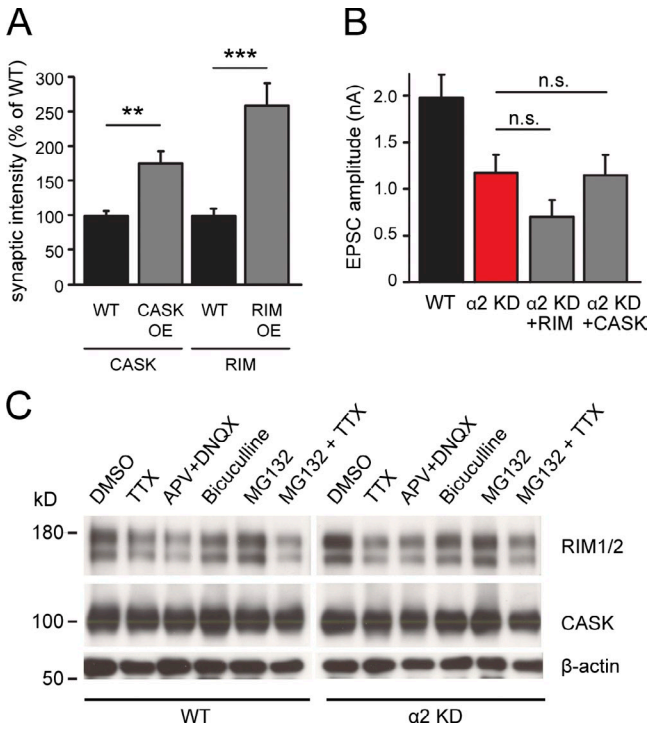

Figure 7. **RIM and CASK overexpression is unable to rescue liprin-α2 phenotype.** (A) Quantification of immunofluorescence intensity of RIM1 and CASK at presynaptic sites infected with lentiviral particles expressing mCherry (WT) or mCherry plus RIM1 or CASK (RIM OE and CASK OE, respectively). Intensity of labeling in control cells was set to 100%. **, $P < 0.01$; ***, $P < 0.001$. (B) Evoked EPSC size in hippocampal autapses infected with liprin shRNA viruses cannot be rescued by overexpression of RIM1-IRES-mCherry or CASK-IRES-mCherry. Neurons were infected at DIV9 and recorded at DIV14 (WT: 1.99 ± 0.25 nA, $n = 24$; α2 KD: 1.18 ± 0.2 nA, $n = 19$; α2 KD + RIM: 0.72 ± 0.17 nA, $n = 10$; α2 KD + CASK: 1.14 ± 0.21 nA, $n = 10$; WT vs. α2 KD: $P = 0.016$; WT vs. α2 KD + RIM1: $P = 0.003$; WT vs. α2KD + CASK: $P = 0.046$; all other combinations: NS, $P > 0.05$, including liprin-α2 shRNA vs. liprin-α2 shRNA + RIM1 [$P = 0.191$]). (C) Western blot of extracts of DIV21 hippocampal neuron cultures. Neurons were infected at DIV15 with liprin-α2 shRNA or scrambled shRNA expressing lentivirus and treated for 48 h with 2 µM TTX, 50 µM APV and 10 µM DNQX, 40 µM Bicuculline, or DMSO (control) or for 6 h with 10 µM MG132. Equal volumes of extracts were loaded and immunoblotted for CASK, RIM1/2, and β-actin as loading control. These results indicate that activity-dependent regulation of RIM1/2 and CASK is not mediated through liprin-α2. Data are presented as mean values ± SEM.

Liprin-α2 controls synaptic protein composition

Changes in SV pools and presynaptic plasticity were accompanied by disrupted localization of important presynaptic proteins in the absence of liprin-α2, and reintroduction of liprin-α2 binding partners RIM1 and CASK could not compensate for the loss of liprin-α2 (Fig. 6). FRAP experiments showed that liprin-α2 controls the dynamics of RIM1 and CASK at presynaptic boutons (Fig. 8) and, combined with the physiology data, suggests that AZ protein mobility is positively correlated with synaptic output. Furthermore, our FRAP analysis suggests that liprin-α2, RIM1, and CASK proteins exist at presynapses in two pools: a relatively small immobile pool and a larger mobile one. Depleting synaptic liprin-α2 by expressing specific shRNA caused a decrease in the mobility of liprin-α2 binding partners RIM1 and CASK, as well as a notable decrease in presynaptic efficacy. Conversely, increasing synaptic liprin-α2, in this case with MG132, resulted in a larger mobile pool of liprin-α2, which is consistent with the reported increased synaptic efficacy upon ubiquitin–proteasome system blockade (Rinetti and Schweizer, 2010). We propose a model in which liprin-α2 functions in regulating the relative sizes of the mobile and immobile fractions of RIM and CASK in synapses, and that proper maintenance of the dynamic fraction is necessary for normal presynaptic output (Fig. 9). Liprin-α2 may regulate RIM1 and CASK dynamics by competing with other RIM1 and CASK interaction partners. Such a competitive model for liprin-α2 is consistent with the numerous interactions between liprin-α2 and other AZ proteins (Schoch and Gundelfinger, 2006; Spangler and Hoogenraad, 2007). In other systems, computational models of protein–protein interaction networks indicate that cooperating and competitive interacting partners strongly increase the dynamics in protein clusters (Kim et al., 2006). Thus, liprin-α2 is not only critically important for synaptic levels of RIM1 and CASK but it also provides dynamic interaction sites for RIM1/CASK and potentially other AZ proteins to maintain synaptic efficacy. Our data suggest that liprin-α2 is a likely candidate to organize presynaptic composition and provides the flexibility needed to maintain the dynamic pool of AZ proteins that facilitates SV release at presynaptic boutons.

Common and diverging properties of liprin-α family proteins

C. elegans and *D. melanagaster* each contain only one liprin-α, SYD-2 and dliprin-α, respectively (Zhen and Jin, 1999; Kaufmann et al., 2002), and vertebrates contain four liprin-α members (Serra-Pagès et al., 1998). Although the vertebrate liprin-α isoforms are highly homologous and have several common properties, each isoform may exhibit functional diversity and perform specific functions. Most of the previous studies are based on overexpression of truncated or mutant forms of liprin-α (Wyszynski et al., 2002; Ko et al., 2003; Dunah et al., 2005; Hoogenraad et al., 2007), making it difficult to draw conclusions about the specific roles of the liprin-α isoforms. Here we used a specific liprin-α2 knockdown approach, which allows us to investigate in a much more precise way the influence of one particular liprin-α isoform. Nevertheless, it is still challenging to dedicate a particular function to liprin-α2 because of several factors. First, it is very likely that there is high functional redundancy between the liprin-α family members for their common properties at the synaptic terminals. For example, liprin-α3 is enriched at synapses in hippocampal neurons (Spangler et al., 2011) and might compensate for some of the liprin-α2 effects. The possible redundancy might be somehow different at pre- and postsynapse, giving a possible explanation for the observed presynaptic effect of liprin-α2 depletion and the lack of a clear postsynaptic phenotype. Second, liprin-αs can form oligomers through both homo- and heterodimerization (Serra-Pagès et al., 1998). Recent structure–function studies demonstrate that the dimerization of SYD-2 promotes a higher order of oligomerization, which is essential for presynaptic formation (Taru and Jin, 2011). However, it remains unclear how deletion of one isoform affects the organization and/or complex formation of the other

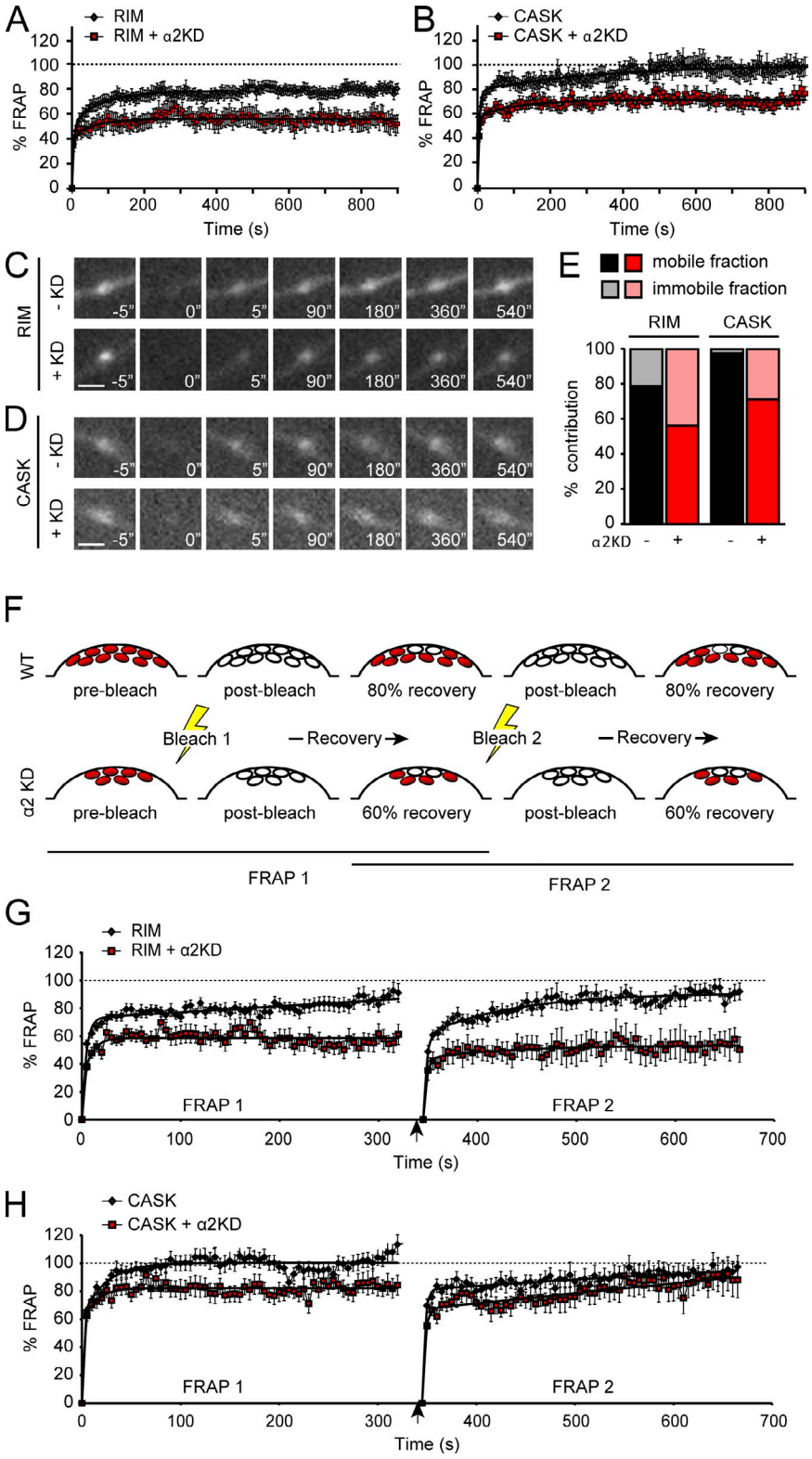

Figure 8. **Liprin-α2 is important for synaptic protein dynamics.** (A) Mean recovery time course of photobleached mCherry-RIM1 in the presence of liprin-α2 shRNA (n = 10 synapses) or control shRNA (n = 16 synapses) in single synapses in DIV15+4 neurons. The data were fitted according to a two-exponential model (black lines). Dashed line indicates 100% recovery. ANOVA repeated measures: F = 5.02, P = 0.034. n = 2 independent experiments. (B) Mean recovery time course of photobleached mCherry-CASK in the presence of liprin-α2 shRNA (n = 16 synapses) or control (n = 22 synapses) in single synapses in DIV15+4 neurons. The data were fitted according to a two-exponential model (black lines). Dashed line indicates 100% recovery. ANOVA repeated measures: P = 0.003, F = 9.83. n = 2 independent experiments. (C) Representative images before and after photobleaching of mCherry-RIM1 in the presence or absence of liprin-α2 shRNA. Bar, 1 µm. (D) Representative images before and after photobleaching of mCherry-CASK in the presence or absence of liprin-α2 shRNA. Bar, 1 µm. (E) Quantification of the mobile and immobile fractions of mCherry-RIM1 or mCherry-CASK in the presence or absence of liprin-α2 shRNA according to the fitted recovery time course after two independent experiments (RIM: −α2KD, mobile: 79%, immobile: 21%; +α2KD, mobile: 56%, immobile: 44%; CASK: −α2KD, mobile: 98%, immobile: 2%; +α2KD, mobile: 71%, immobile: 29%). (F) Schematic representation of a dual FRAP experiment including a second photobleach event of mCherry-RIM1 in the presence (bottom) or absence (top) of liprin-α2 shRNA. Fluorescent-tagged RIM1 (red ovals) are photobleached (white ovals) and fluorescent recovery is monitored. After a plateau is reached, a second photobleach was applied and fluorescent recovery was measured. (G) Mean recovery time course of photobleached mCherry-RIM1 in single synapses in the presence of liprin-α2 shRNA (n = 40 synapses) or control shRNA (n = 46 synapses). After 345 s a second photobleach was applied, indicated by an arrow. n = 3. Data were fit according to a two-exponential model (black lines). Dashed line indicates 100% recovery. FRAP1: F = 14.92, P < 0.0005; FRAP2: F = 1.77, P = 0.188. ANOVA repeated measures: n = 3 independent experiments. (H) Mean recovery time course of photobleached mCherry-CASK in single synapses in the presence of liprin-α2 shRNA (n = 34 synapses) or control shRNA (n = 38 synapses). After 345 s a second photobleach was applied, indicated by an arrow. n = 3. Data were fit according to a two-exponential model (black lines). Dashed line indicates 100% recovery. FRAP1: F = 7.76, P = 0.007; FRAP2: F = 1.14, P = 0.291. ANOVA repeated measures: n = 3 independent experiments. Data are presented as mean values ± SEM.

liprins at synapses. Third, small amino acid sequence divergences could be responsible for functional differences between the liprin-α isoforms (Spangler and Hoogenraad, 2007; Spangler et al., 2011). For example, the major liprin-α4 splice variant lacks the C-terminal PDZ binding motif, which is present in all other liprin-α isoforms (Zürner et al., 2011). Moreover, cellular, structural, and biochemical data demonstrated that CASK binds to liprin-α2 and not to liprin-α1 (Wei et al., 2011). The interaction of liprin-α2 (and α3 and α4) with CASK depends on a 37–amino acid sequence insertion between the SAM1 and SAM2 domains. Additional studies are required to determine whether additional sequence divergence is responsible for some of the functional differences and whether other synaptic proteins interact with particular liprin-α isoforms.

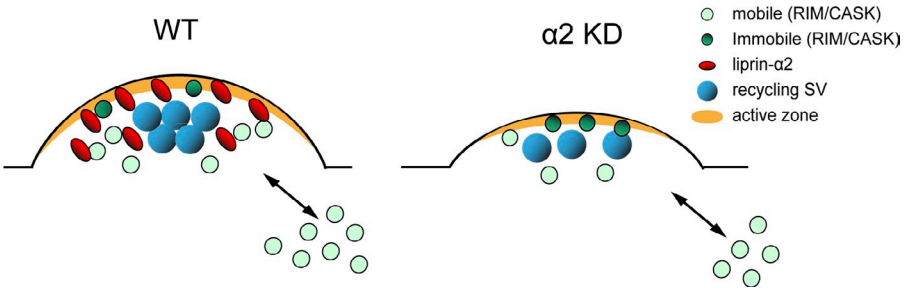

Figure 9. **Model of liprin-α2 in modulating AZ dynamics.** Liprin-α2 (red) organizes presynaptic ultrastructure and controls synaptic output by regulating the size of the recycling pool of SVs (blue) via recruitment of several components of the release machinery, including RIM1 and CASK (green). Depletion of synaptic liprin-α2 reorganizes presynaptic structure and compositions and causes a decrease in the mobility of liprin-α2 binding partners RIM1 and CASK, as well as a notable decrease in presynaptic efficacy. Liprin-α2 may function in regulating the relative sizes of the mobile (light green) and immobile (dark green) fractions, and thereby the dynamics of RIM and CASK in synapses, by competing with other RIM1 and CASK interaction partners. Liprin-α2 provides dynamic interaction sites for RIM1/CASK and potentially other AZ proteins to maintain synaptic efficacy.

This is the first study to show that liprin-α family proteins have a presynaptic function in vertebrates as proposed in the invertebrate genetic models of *D. melanogaster* and *C. elegans* and unmasks a functional role for the liprin-α2 isoform at mature presynaptic terminals. Our data suggest a model wherein liprin-α2 plays an important role in organizing presynaptic composition and promotes AZ dynamics and thereby synaptic output. We propose that liprin-α2 is a unique adaptor protein that increases AZ dynamics rather than merely anchoring and stabilizing synaptic protein complexes. Activity-dependent manipulation of liprin-α2 levels via the proteasome system may serve as a mechanism to regulate protein dynamics at the AZ and tune synaptic efficacy during periods of high neuronal activity.

Materials and methods

Animals

All animal experiments were performed in compliance with the guidelines for the welfare of experimental animals issued by the federal government of the Netherlands. All animal experiments were approved by the Animal Ethical Review Committee of the Erasmus Medical Center, Utrecht University or VU University Amsterdam.

Antibodies, reagents, DNA constructs, and siRNAs

The rabbit polyclonal anti–liprin-α2 antibodies were raised against amino acids 498–635 (NCBI Nucleotide accession no. NM_003625.2; see Table S3). All other antibodies and reagents that were used are indicated in Tables S3 and S4. The following mammalian expression plasmids have been described previously: pGW1-GFP and pβactin-HA-β-galactosidase (Hoogenraad et al., 2005), biotin-tag-GFP vector and HA-BirA (Jaworski et al., 2009), and pSuper vector (Brummelkamp et al., 2002). The liprin-α expression constructs were generated by a PCR-based strategy using human liprin-α1 and human liprin-α2 cDNA (Serra-Pagès et al., 1998) and subcloned in pGW1, pGW2, and pβactin expression vectors (Kapitein et al., 2010) using the AscI–EcoRI or EcoRI sites, respectively. In bio-GFP-liprin-α2 fusions, a linker encoding the sequence MASGLNDIFEAQKIEWHEGGG, which is the substrate of biotin ligase BirA, was inserted into the NheI and AgeI sites in front of the pEGFP-C2 (Takara Bio, Inc.) and the liprin-α2 open reading frame subsequently subcloned in the biotin-tag-GFP vector. CASK and RIM1 cDNAs were gifts of T. Südhof (Stanford University, Stanford, CA) and were cloned into pLenti_ires_mCherry vectors (Wierda et al., 2007). SyPhy cDNA was a gift of L. Lagnado (Medical Research Council, Cambridge, UK).

The following shRNA sequences were used (see also Table S1): liprin-α1 (5′-TCTGTGCATGACCTCAATG-3′), liprin-α2#1 (5′-GCATGAACTTCTTGAAGAA-3′), liprin-α2#2 (5′-AGCCAGTCTGATTACAGAA-3′), and CASK (5′-GCACTGAATCACCCATGGC-3′). shRNA sequences targeting rat liprin-α1 (NCBI Nucleotide accession no. NM_001106320.2), liprin-α2 (NCBI Nucleotide accession no. NM_001108745.1), and CASK mRNA (NCBI Nucleotide accession no. U47110) were designed using the siRNA selection program at OligoEngine. CAST2/ERC1 (5′-ATGCTGCCTATGCTACATC-3′), CAST1/ERC2 (5′-CATCAACAACTTACCCAAA-3′), and RIM1 (5′-AGTCCAGACGGTAAAGTTC-3′) shRNA were designed using the selection program at the Whitehead Institute (http://sirna.wi.mit.edu/). Bassoon (5′-AACACCTGCACCCAGTGTCAC-3′) and piccolo (5′-AAGTGCTGTCTCCTCTGTTGT-3′) shRNA were based on published sequences (Leal-Ortiz et al., 2008). The complementary oligonucleotides were annealed and inserted into pSuper vector (Brummelkamp et al., 2002). Liprin-α1 and liprin-α2 shRNA lentiviral constructs were created by inserting the N1 promoter and the aforementioned shRNA sequences into the XbaI and XhoI sites of pLenti-Lox3.7, which contained EGFP driven by a human synapsin1 promoter (Rubinson et al., 2003).

Primary hippocampal neuron cultures, transfection, immunofluorescent staining, and fixed imaging

Primary hippocampal cultures were prepared from embryonic day 18 rat brains. Cells were plated on coverslips coated with 30 µg/ml poly-L-lysine and 2 µg/ml laminin at a density of 75,000/well (mass cultures). Hippocampal cultures were grown in neurobasal medium (NB) supplemented with B27, 0.5 mM glutamine, 12.5 µM glutamate, and penicillin/streptomycin (Spangler et al., 2011). Hippocampal neurons were transfected using Lipofectamine 2000 (Invitrogen). In brief, DNA (3.6 µg/well) was mixed with 3 µl Lipofectamine 2000 in 200 µl NB, incubated for 30 min, and then added to the neurons in NB at 37°C in 5% CO_2 for 45 min. Next, neurons were washed with NB and transferred in the original medium at 37°C in 5% CO_2 for 2–4 d.

For immunofluorescent stainings, neurons were fixed for 10 min with 4% paraformaldehyde/4% sucrose in PBS or 10 min with ice-cold 100% methanol/1 mM EGTA at −20°C. After fixation, cells were washed three times in PBS for 5 min at room temperature, and incubated with primary antibodies in GDB buffer (0.2% BSA, 0.8 M NaCl, 0.5% Triton X-100, and 30 mM phosphate buffer, pH 7.4) overnight at 4°C. Neurons were then washed three times in PBS for 5 min at room temperature and incubated with Alexa-conjugated secondary antibodies in GDB for 2 h at room temperature and washed three times in PBS for 5 min. Slides were mounted using Vectashield mounting medium (Vector Laboratories).

Confocal images were acquired using a confocal laser-scanning microscope (LSM510; Carl Zeiss) with a 40× 1.3 NA or 63× 1.4 NA oil objective. Each image was a z-series of 10–12 images, each averaged two times and was chosen to cover the entire region of interest from top to bottom. The resulting z-stack was flattened into a single image using maximum projection. Images were not further processed and were of similar high quality to the original single planes. Confocal settings were kept the same for all scans when fluorescence intensity was compared. Morphometric analysis, quantification, and colocalization were performed using MetaMorph software (Molecular Devices).

Time-lapse live imaging, SV exocytosis, and FRAP experiments

Time-lapse live-cell imaging was performed on an inverted research microscope (Eclipse TE2000E; Nikon) with a CFI Apo total internal reflection microscopy 100× 1.49 NA oil objective (Nikon), equipped with Coolsnap and QuantEM EMCCD cameras (Roper Scientific) controlled by MetaMorph 7.1 software. For SV exocytosis experiments, we used a HBO 103 W/2 Mercury Short Arc Lamp (Osram) and a Chroma ETGFP/mCherry filter cube

for excitation. To separate emissions we used DualView (Optical Insight) with emitters HQ530/30M and HQ630/50M (Chroma Technology Corp.) and the beam splitter 565DCXR (Chroma Technology Corp.). For FRAP experiments, cells were imaged with total internal reflection microscopy using a 488- or 561-nm laser. During imaging, cells were maintained at 37°C in either Tyrode solution (2.5 mM KCl, 119 mM NaCl, 25 mM Hepes, 30 mM glucose, 2 mM $CaCl_2$, and 2 mM $MgCl_2$), for SV exocytosis experiments, or the standard culture medium, for FRAP experiments, in a closed chamber with 5% CO_2 (model INUG2-ZILCS-H2; Tokai Hit).

For SV exocytosis experiments using FM dyes, neurons were transfected at DIV15 and loaded with 10 µM FM4-64FX (Invitrogen) at DIV19 (Fernández-Alfonso and Ryan, 2004) and areas containing transfected axons were selected. One image of the FM4-64–loaded synapses was taken before the second stimulation, and images were acquired at an interval of ∼7 s for 2 min immediately after the second stimulation.

For SV exocytosis experiments using SyPhy (Granseth et al., 2006), hippocampal mass cultures were transfected with SyPhy and ECFP at DIV10 and imaged at DIV15. Neurons were stimulated by 200 AP at 20 Hz using field stimulation via platinum electrodes passing 1-ms, 30-mA currents. Calcium imaging using Fluo-4 (Invitrogen) measurements was used to confirm that each stimulus triggered an action potential. Neurons were perfused (0.2 ml/min) in a saline solution containing 119 mM NaCl, 2.5 mM KCl, 2 mM $CaCl_2$, 2 mM $MgCl_2$, 25 mM Hepes (buffered to pH 7.4), 30 mM glucose, 10 mM 6-cyano-7-nitroquinoxaline-2,3-dione, and 50 mM D, L-2-amino-5-phosphonovaleric acid (AP5) at 24°C. NH_4Cl application was done with 50 mM NH_4Cl substituting 50 mM NaCl (buffered to pH 7.4).

FRAP experiments were performed using the FRAP scanning head 3 FRAP L5 D-CURIE (Curie Institute) and the 488- or 561-nm laser line for bleaching. To analyze the recovery of fluorescence, areas including the bleached synapse were selected and background subtracted frame by frame by subtracting the mean intensity of an empty, nonbleached area. FRAP data were normalized and corrected for ongoing photobleaching. Recovery R was then calculated as R = [I(t) − I(directly after bleaching)]/[I(before bleaching) − I(directly after bleaching)], with I denoting total synapse intensity. FRAP recovery curves were fit using a two-exponential model in SigmaPlot and the final recovery Rfinal for each individual trace was determined as the level of the fitted recovery curve at the end of the recording. The immobile fraction was then calculated as 1-Rfinal. The recovery half-time was determined for each trace as the first time point where recovery reached the level corresponding to half the final recovery. Analysis was performed using MetaMorph software and statistical significance was measured by analysis of variance (ANOVA) repeated measurements in SPSS 16.0 (SPSS, Inc.).

Autaptic cultures and virus infection

A thin layer of agarose was applied to glass coverslips to prevent cell adhesion. Agarose-covered coverslips were stamped with a mixture of 0.1 mg/ml poly-D-lysine (Sigma-Aldrich) and 0.2mg/ml rat-tail collagen (BD) solution using a custom made rubber stamp (Toonen et al., 2006; Wierda et al., 2007; Weber et al., 2010). Coverslips were UV sterilized for 20 min before and after stamping. Primary rat astrocytes were plated at a density of 8,000/well and were allowed to form micro islands for 4–6 d in DMEM supplemented with 10% FCS, 1% nonessential amino acids, and 1% penicillin/streptomycin (Wierda et al., 2007).

Isolated hippocampal rat neurons were plated on astrocyte micro islands at a density of 2,000 cells/well and were grown in NB (Invitrogen) supplemented with 2% B-27 (Invitrogen), 1.8% Hepes, 0.25% glutamax (Invitrogen), and 0.1% Pen/Strep (Invitrogen; Wierda et al., 2007). Generally, cells were infected with lentiviral vectors containing either GFP as control or GFP and liprin shRNAs at DIV9. Only islands containing single neurons were examined at DIV14–17.

Electrophysiological recordings

Electrophysiological recordings were performed on DIV14–17 autaptic glutamatergic hippocampal neurons at room temperature (±21°C; Toonen et al., 2006; Wierda et al., 2007). Whole cell voltage-clamp (V_m = −70 mV) recordings were acquired with an Axopatch 200A amplifier, Digidata 1322A, and Clampex 9.0 software. Recordings were performed at DIV14–17 with borosilicate glass pipettes (2.5–4 mOhm) containing 125 mM potassium-gluconate, 10 mM NaCl, 4.6 mM $MgCl_2$, 4 mM K_2-ATP, 1 mM EGTA, 15 mM creatine phosphate, and 20 U/ml phosphocreatine kinase (pH 7.30; 300 mOsm). The external medium contained 140 mM NaCl, 2.4 mM KCl, 4 mM $CaCl_2$, 4 mM $MgCl_2$, 10 mM Hepes, and 10 mM glucose (pH 7.30; 300 mosm). After whole cell mode was established, only cells with an access resistance of <10 MΩ and leak current of <300 pA were accepted for analysis. Hypertonic sucrose (500 mM) was applied using a fast barrel application system (Perfusion Fast-Step; Warner Instruments) to assess RRP size. P_{vr} was calculated as the response to a single stimulus divided by the response to hypertonic sucrose. All recordings were performed at room temperature. Analysis was performed using Clampfit v9.0 (Axon Instruments), Mini Analysis Program v6.0 (Synaptosoft), and custom-written software routines in Matlab 7.1 or R2009b (MathWorks).

Biotin-streptavidin pull-down experiments and mass spectrometry analysis

Streptavidin bead pull-down assays were performed as previously described (Jaworski et al., 2009). HEK293 cells were transfected with BirA and bio-GFP-liprin-α2 or bio-GFP using Lipofectamine 2000 transfection reagent according to the manufacturer's instructions. Cells were lysed 16 h later in 20 mM Tris-HCl, pH 8.0, 150 mM KCl, 1% Triton X-100, and protease inhibitors (Roche). Cell lysates were centrifuged at 13,000 rpm for 10 min and the supernatants were incubated with Dynabeads M-280 streptavidin (Invitrogen) for 30 min. Beads were separated by using a magnet (Invitrogen) and washed two times in low salt wash buffer (20 mM Tris-HCl, pH 8.0, 100 mM KCl, and 0.1% Triton X-100), two times in high salt wash buffer (20 mM Tris-HCl, pH 8.0, 500 mM KCl, and 0.1% Triton X-100), and two more times in low salt wash buffer to remove binding proteins from HEK cells. P2 fractions from adult female rat brains were isolated and extracted with 1% sodium deoxycholate (DOC) in 500 mM Tris, pH 9.0, by incubation for 30 min at 36°C (Lee et al., 2001). Extracts were dialyzed overnight into a 50mM Tris (pH 7.4)/0.1% Triton X-100 solution and spun down at 13,200 rpm for 40 min. The resulting supernatant is referred to as the P2/DOC extract and was incubated with the Dynabeads containing bio-liprin-α2 or bio-GFP for 2 h at 4°C and washed with low salt wash buffer three times. For protein elution, the beads were boiled in NuPAGE LDS 4 sample buffer (Invitrogen) and separated, and supernatants were run on a 4–12% NuPAGE tris-acetate gel (Invitrogen). The gel was stained with the colloidal blue staining kit (Invitrogen).

For mass spectrometry analysis, 1D SDS-PAGE gel lanes were cut into 2-mm slices using an automatic gel slicer and subjected to in-gel reduction with dithiothreitol, alkylation with iodoacetamide, and digestion with trypsin (Jaworski et al., 2009). Nanoflow LCMS/MS was performed on an 1100 series capillary LC system (Agilent Technologies) coupled to an LTQ linear ion trap mass spectrometer (Thermo Fisher Scientific) operating in positive mode and equipped with a nanospray source. The Mascot search algorithm (version 2.2) was used for searching against the International Protein Index database (release number IPI_rat_20100507.fasta or IPI_human_20100507.fasta). The Mascot score cut-off value for a positive protein hit was set to 60. Individual peptide MS/MS spectra with Mowse scores <40 were checked manually and either interpreted as valid identifications or discarded. Proteins present in the negative controls (pull-down assays with bioGFP alone) were omitted from Table S2.

Image analysis and quantification

Morphometric analyses of hippocampal neurons. Synapse size in dissociated hippocampal neurons was determined by cotransfection of soluble mCherry to fill the cell. The mean pixel length and height per synapse were measured using MetaMorph software on the z-section where the synapse appeared largest.

Quantification of synaptic targeting at presynaptic boutons. For analysis of presynaptic boutons we used GFP as an unbiased cell-fill. Because axons often crossed several z planes, we took series stacks from the bottom to the top of all axons and used the LSM software to generate image projections for quantitative analyses. Presynaptic boutons were morphologically identified as swellings along GFP-labeled axon (Bamji et al., 2003; Leal-Ortiz et al., 2008). Hippocampal neurons were transfected with a plasmid encoding GFP at DIV15 and stained after 4 d with antibodies for several presynaptic proteins. As shown in Fig. S2, GFP-positive axon segments exhibit axonal varicosities that reliably colocalized with presynaptic marker VAMP2. To control for background and false positive colocalization at presynaptic boutons, we rotated the red-channel image of the VAMP2 staining by 90° and 180° and found that ∼20% of synaptic staining at axonal swelling is a result of coincidental crossing or overlap of nontransfected axons in the culture (Fig. S2 B). Quantification demonstrated that ∼80% of these swellings were positive for endogenous presynaptic proteins (Fig. S2 C). For quantitative analysis of synaptic targeting, 20 GFP-positive presynaptic boutons were blindly selected from each confocal image and quantified for presence or absence of synaptic protein staining. All results were verified in at least two independent experiments ($n > 5$ for individual experiments). Statistical analysis was performed with Student's *t* test assuming two-tailed

distribution and unequal variation. *n* was defined as the number of transfected cells.

Quantification of fluorescent intensity. Images of dissociated hippocampal neurons were analyzed using MetaMorph software. Presynaptic boutons were morphologically identified as swellings along GFP-labeled axon segments as described or by colocalization with PSD-95 and bassoon. Fluorescence intensities were measured using confocal images taken with identical laser power and microscope settings. A region was drawn around each synapse and the mean intensity within the region was measured, corrected for background staining, and normalized to nontransfected neurons in the same field. Images of autaptic neurons were analyzed in Matlab with SynD (Schmitz et al., 2011). Dendrites were detected based on the staining for MAP2 or GFP expression. Synapses were detected based on the staining for VAMP or Synapsin. Detected synapses mask was used to measure the synaptic intensity of additional proteins. Measurements of FM4-64 recycling at presynaptic boutons were performed as described previously (Murthy et al., 1997). Synapses from >5 neurons per experiment were identified in MetaMorph by morphology and overlaid onto the FM4-64 images for quantification of fluorescence intensity using MetaMorph software. The intensity of all points after unloading was normalized to the intensity of that synapse before unloading. Separate experiments were adjusted to control to allow for comparison and analyzed in a blind manner. Statistical significance was measured by ANOVA repeated measurements in SPSS 16.0. Measurements of SyPhy fluorescence at individual boutons were performed as described previously (Granseth et al., 2006). The peak of amplitude at 200 AP was selected at the end of the stimulation. Maximal mean value of SyPhy fluorescence upon NH_4Cl superfusion was used to normalize SyPhy fluorescence upon AP stimulation at individual synapses.

Data representation and statistics

In all bar graphs, data are presented as mean values ± SEM. Statistical analysis was performed with SigmaPlot v11.0 (Systat Software) or SPSS 16.0. Data samples were tested for normal distribution with the Kolmogorov and Smirnov test and for heterogeneity of variance with the method of Barlett. If allowed, an unpaired *t* test (with Welch correction if required) was used. Alternatively, the nonparametric Mann-Whitney *U* test was used to test for statistical significance. For multiple groups, one-way ANOVA or the nonparametric Kruskal-Wallis test was used. P-values below 0.05 are considered significant (*, $P < 0.05$; **, $P < 0.01$; and ***, $P < 0.001$).

Online supplemental material

Fig. S1 shows the electrophysiological parameters of a second independent liprin-α2 shRNA, liprin-α1 shRNA, and a liprin-α2 shRNA-resistant rescue construct. Fig. S2 shows the method used for quantifying the localization of presynaptic proteins. Table S1 shows the pSuper-shRNA sequences tested and used in the study. Table S2 shows the binding partners of liprin-α2 in rat brain extracts identified by mass spectrometry. Table S3 shows the antibodies used in this study and Table S4 shows the reagents used in this study. Online supplemental material is available at http://www.jcb.org/cgi/content/full/jcb.201301011/DC1.

We thank Robbert Zalm, Desiree Schut, and Ingrid Saarloos for expert technical assistance with lentivirus production and autaptic cultures and Rien Dekker for electron microscopy.

This work is supported by the Netherlands Organization for Scientific Research (NWO-ALW-VICI and NWO-CW-ECHO; ZonMw-TOP to C.C. Hoogenraad; ZonMw-VENI and ZonMw-TOP to R.F. Toonen; and ZonMw-VIDI to E. de Graaff), Neuromics Marie Curie Early stage Training grant (MEST-CT-2005-020919 to S.K. Schmitz), European Science Foundation (European Young Investigators Award to C.C. Hoogenraad), and Human Frontier Science Program Career Development Award (to C.C. Hoogenraad). S.K. Schmitz is a recipient of the Netherlands Scientific Organization Toptalent grant (NWO 021.001.076).

The authors declare no competing financial interests.

Author contributions: S.A. Spangler, S.K. Schmitz, J.T. Kevenaar, R.F. Toonen, and C.C. Hoogenraad designed the research; S.A. Spangler, R.F. Toonen, and J.T. Kevenaar generated liprin-α constructs and performed biochemistry, immunocytochemistry, and live imaging experiments; S.K. Schmitz performed electrophysiological recordings, autapse immunocytochemistry, and biochemistry experiments; E. de Graaff made lentiviral constructs; H. de Wit supervised electron microscopy; J. Demmers performed mass spectrometry; S.A. Spangler, S.K. Schmitz, R.F. Toonen, and J.T. Kevenaar analyzed the data; and S.A. Spangler, R.F. Toonen, and C.C. Hoogenraad wrote the manuscript with the help of all others.

Submitted: 3 January 2013
Accepted: 2 May 2013

References

Astigarraga, S., K. Hofmeyer, R. Farajian, and J.E. Treisman. 2010. Three *Drosophila* liprins interact to control synapse formation. *J. Neurosci.* 30:15358–15368. http://dx.doi.org/10.1523/JNEUROSCI.1862-10.2010

Atwood, H.L., and S. Karunanithi. 2002. Diversification of synaptic strength: presynaptic elements. *Nat. Rev. Neurosci.* 3:497–516. http://dx.doi.org/10.1038/nrn876

Bamji, S.X., K. Shimazu, N. Kimes, J. Huelsken, W. Birchmeier, B. Lu, and L.F. Reichardt. 2003. Role of beta-catenin in synaptic vesicle localization and presynaptic assembly. *Neuron*. 40:719–731. http://dx.doi.org/10.1016/S0896-6273(03)00718-9

Bingol, B., and M. Sheng. 2011. Deconstruction for reconstruction: the role of proteolysis in neural plasticity and disease. *Neuron*. 69:22–32. http://dx.doi.org/10.1016/j.neuron.2010.11.006

Brummelkamp, T.R., R. Bernards, and R. Agami. 2002. A system for stable expression of short interfering RNAs in mammalian cells. *Science*. 296:550–553. http://dx.doi.org/10.1126/science.1068999

Calakos, N., S. Schoch, T.C. Südhof, and R.C. Malenka. 2004. Multiple roles for the active zone protein RIM1alpha in late stages of neurotransmitter release. *Neuron*. 42:889–896. http://dx.doi.org/10.1016/j.neuron.2004.05.014

Chia, P.H., M.R. Patel, and K. Shen. 2012. NAB-1 instructs synapse assembly by linking adhesion molecules and F-actin to active zone proteins. *Nat. Neurosci.* 15:234–242. http://dx.doi.org/10.1038/nn.2991

Choe, K.M., S. Prakash, A. Bright, and T.R. Clandinin. 2006. Liprin-alpha is required for photoreceptor target selection in *Drosophila*. *Proc. Natl. Acad. Sci. USA*. 103:11601–11606. http://dx.doi.org/10.1073/pnas.0601185103

Dai, Y., H. Taru, S.L. Deken, B. Grill, B. Ackley, M.L. Nonet, and Y. Jin. 2006. SYD-2 Liprin-alpha organizes presynaptic active zone formation through ELKS. *Nat. Neurosci.* 9:1479–1487. http://dx.doi.org/10.1038/nn1808

Dunah, A.W., E. Hueske, M. Wyszynski, C.C. Hoogenraad, J. Jaworski, D.T. Pak, A. Simonetta, G. Liu, and M. Sheng. 2005. LAR receptor protein tyrosine phosphatases in the development and maintenance of excitatory synapses. *Nat. Neurosci.* 8:458–467.

Fernández-Alfonso, T., and T.A. Ryan. 2004. The kinetics of synaptic vesicle pool depletion at CNS synaptic terminals. *Neuron*. 41:943–953. http://dx.doi.org/10.1016/S0896-6273(04)00113-8

Gekel, I., and E. Neher. 2008. Application of an Epac activator enhances neurotransmitter release at excitatory central synapses. *J. Neurosci.* 28:7991–8002. http://dx.doi.org/10.1523/JNEUROSCI.0268-08.2008

Granseth, B., B. Odermatt, S.J. Royle, and L. Lagnado. 2006. Clathrin-mediated endocytosis is the dominant mechanism of vesicle retrieval at hippocampal synapses. *Neuron*. 51:773–786. http://dx.doi.org/10.1016/j.neuron.2006.08.029

Hofmeyer, K., C. Maurel-Zaffran, H. Sink, and J.E. Treisman. 2006. Liprin-alpha has LAR-independent functions in R7 photoreceptor axon targeting. *Proc. Natl. Acad. Sci. USA*. 103:11595–11600. http://dx.doi.org/10.1073/pnas.0604766103

Hoogenraad, C.C., A.D. Milstein, I.M. Ethell, M. Henkemeyer, and M. Sheng. 2005. GRIP1 controls dendrite morphogenesis by regulating EphB receptor trafficking. *Nat. Neurosci.* 8:906–915. http://dx.doi.org/10.1038/nn1487

Hoogenraad, C.C., M.I. Feliu-Mojer, S.A. Spangler, A.D. Milstein, A.W. Dunah, A.Y. Hung, and M. Sheng. 2007. Liprinalpha1 degradation by calcium/calmodulin-dependent protein kinase II regulates LAR receptor tyrosine phosphatase distribution and dendrite development. *Dev. Cell*. 12:587–602. http://dx.doi.org/10.1016/j.devcel.2007.02.006

Jaworski, J., L.C. Kapitein, S.M. Gouveia, B.R. Dortland, P.S. Wulf, I. Grigoriev, P. Camera, S.A. Spangler, P. Di Stefano, J. Demmers, et al. 2009. Dynamic microtubules regulate dendritic spine morphology and synaptic plasticity. *Neuron*. 61:85–100. http://dx.doi.org/10.1016/j.neuron.2008.11.013

Kalla, S., M. Stern, J. Basu, F. Varoqueaux, K. Reim, C. Rosenmund, N.E. Ziv, and N. Brose. 2006. Molecular dynamics of a presynaptic active zone protein studied in Munc13-1-enhanced yellow fluorescent protein knock-in mutant mice. *J. Neurosci.* 26:13054–13066. http://dx.doi.org/10.1523/JNEUROSCI.4330-06.2006

Kapitein, L.C., K.W. Yau, and C.C. Hoogenraad. 2010. Microtubule dynamics in dendritic spines. *Methods Cell Biol.* 97:111–132. http://dx.doi.org/10.1016/S0091-679X(10)97007-6

Kaufmann, N., J. DeProto, R. Ranjan, H. Wan, and D. Van Vactor. 2002. *Drosophila* liprin-alpha and the receptor phosphatase Dlar control synapse morphogenesis. *Neuron*. 34:27–38. http://dx.doi.org/10.1016/S0896-6273(02)00643-8

Kim, P.M., L.J. Lu, Y. Xia, and M.B. Gerstein. 2006. Relating three-dimensional structures to protein networks provides evolutionary insights. *Science*. 314:1938–1941. http://dx.doi.org/10.1126/science.1136174

Ko, J., S. Kim, J.G. Valtschanoff, H. Shin, J.R. Lee, M. Sheng, R.T. Premont, R.J. Weinberg, and E. Kim. 2003. Interaction between liprin-alpha and GIT1 is required for AMPA receptor targeting. *J. Neurosci.* 23:1667–1677.

Lazarevic, V., C. Schöne, M. Heine, E.D. Gundelfinger, and A. Fejtova. 2011. Extensive remodeling of the presynaptic cytomatrix upon homeostatic adaptation to network activity silencing. *J. Neurosci.* 31:10189–10200. http://dx.doi.org/10.1523/JNEUROSCI.2088-11.2011

Leal-Ortiz, S., C.L. Waites, R. Terry-Lorenzo, P. Zamorano, E.D. Gundelfinger, and C.C. Garner. 2008. Piccolo modulation of Synapsin1a dynamics regulates synaptic vesicle exocytosis. *J. Cell Biol.* 181:831–846. http://dx.doi.org/10.1083/jcb.200711167

Lee, S.H., J.G. Valtschanoff, V.N. Kharazia, R. Weinberg, and M. Sheng. 2001. Biochemical and morphological characterization of an intracellular membrane compartment containing AMPA receptors. *Neuropharmacology*. 41:680–692. http://dx.doi.org/10.1016/S0028-3908(01)00124-1

Lippincott-Schwartz, J., N. Altan-Bonnet, and G.H. Patterson. 2003. Photobleaching and photoactivation: following protein dynamics in living cells. *Nat. Cell Biol.* Suppl:S7–S14.

Matz, J., A. Gilyan, A. Kolar, T. McCarvill, and S.R. Krueger. 2010. Rapid structural alterations of the active zone lead to sustained changes in neurotransmitter release. *Proc. Natl. Acad. Sci. USA*. 107:8836–8841. http://dx.doi.org/10.1073/pnas.0906087107

Miller, K.E., J. DeProto, N. Kaufmann, B.N. Patel, A. Duckworth, and D. Van Vactor. 2005. Direct observation demonstrates that Liprin-alpha is required for trafficking of synaptic vesicles. *Curr. Biol.* 15:684–689. http://dx.doi.org/10.1016/j.cub.2005.02.061

Murthy, V.N., T.J. Sejnowski, and C.F. Stevens. 1997. Heterogeneous release properties of visualized individual hippocampal synapses. *Neuron*. 18:599–612. http://dx.doi.org/10.1016/S0896-6273(00)80301-3

Owald, D., O. Khorramshahi, V.K. Gupta, D. Banovic, H. Depner, W. Fouquet, C. Wichmann, S. Mertel, S. Eimer, E. Reynolds, et al. 2012. Cooperation of Syd-1 with Neurexin synchronizes pre- with postsynaptic assembly. *Nat. Neurosci.* 15:1219–1226. http://dx.doi.org/10.1038/nn.3183

Patel, M.R., E.K. Lehrman, V.Y. Poon, J.G. Crump, M. Zhen, C.I. Bargmann, and K. Shen. 2006. Hierarchical assembly of presynaptic components in defined *C. elegans* synapses. *Nat. Neurosci.* 9:1488–1498. http://dx.doi.org/10.1038/nn1806

Rinetti, G.V., and F.E. Schweizer. 2010. Ubiquitination acutely regulates presynaptic neurotransmitter release in mammalian neurons. *J. Neurosci.* 30:3157–3166. http://dx.doi.org/10.1523/JNEUROSCI.3712-09.2010

Rosenmund, C., and C.F. Stevens. 1996. Definition of the readily releasable pool of vesicles at hippocampal synapses. *Neuron*. 16:1197–1207. http://dx.doi.org/10.1016/S0896-6273(00)80146-4

Rubinson, D.A., C.P. Dillon, A.V. Kwiatkowski, C. Sievers, L. Yang, J. Kopinja, D.L. Rooney, M. Zhang, M.M. Ihrig, M.T. McManus, et al. 2003. A lentivirus-based system to functionally silence genes in primary mammalian cells, stem cells and transgenic mice by RNA interference. *Nat. Genet.* 33:401–406. (published erratum appears in *Nat. Genet.* 2007. 39:803) http://dx.doi.org/10.1038/ng1117

Schikorski, T., and C.F. Stevens. 1997. Quantitative ultrastructural analysis of hippocampal excitatory synapses. *J. Neurosci.* 17:5858–5867.

Schikorski, T., and C.F. Stevens. 1999. Quantitative fine-structural analysis of olfactory cortical synapses. *Proc. Natl. Acad. Sci. USA*. 96:4107–4112. http://dx.doi.org/10.1073/pnas.96.7.4107

Schmitz, S.K., J.J. Hjorth, R.M. Joemai, R. Wijntjes, S. Eijgenraam, P. de Bruijn, C. Georgiou, A.P. de Jong, A. van Ooyen, M. Verhage, et al. 2011. Automated analysis of neuronal morphology, synapse number and synaptic recruitment. *J. Neurosci. Methods*. 195:185–193. (published erratum appears in *J. Neurosci. Methods.* 2011. 197:190) http://dx.doi.org/10.1016/j.jneumeth.2010.12.011

Schoch, S., and E.D. Gundelfinger. 2006. Molecular organization of the presynaptic active zone. *Cell Tissue Res.* 326:379–391. http://dx.doi.org/10.1007/s00441-006-0244-y

Schoch, S., P.E. Castillo, T. Jo, K. Mukherjee, M. Geppert, Y. Wang, F. Schmitz, R.C. Malenka, and T.C. Südhof. 2002. RIM1alpha forms a protein scaffold for regulating neurotransmitter release at the active zone. *Nature*. 415:321–326. http://dx.doi.org/10.1038/415321a

Serra-Pagès, C., Q.G. Medley, M. Tang, A. Hart, and M. Streuli. 1998. Liprins, a family of LAR transmembrane protein-tyrosine phosphatase-interacting proteins. *J. Biol. Chem.* 273:15611–15620. http://dx.doi.org/10.1074/jbc.273.25.15611

Spangler, S.A., and C.C. Hoogenraad. 2007. Liprin-alpha proteins: scaffold molecules for synapse maturation. *Biochem. Soc. Trans.* 35:1278–1282. http://dx.doi.org/10.1042/BST0351278

Spangler, S.A., D. Jaarsma, E. De Graaff, P.S. Wulf, A. Akhmanova, and C.C. Hoogenraad. 2011. Differential expression of liprin-α family proteins in the brain suggests functional diversification. *J. Comp. Neurol.* 519:3040–3060. http://dx.doi.org/10.1002/cne.22665

Südhof, T.C. 2012. The presynaptic active zone. *Neuron*. 75:11–25. http://dx.doi.org/10.1016/j.neuron.2012.06.012

Tai, H.C., and E.M. Schuman. 2008. Ubiquitin, the proteasome and protein degradation in neuronal function and dysfunction. *Nat. Rev. Neurosci.* 9:826–838. http://dx.doi.org/10.1038/nrn2499

Taru, H., and Y. Jin. 2011. The Liprin homology domain is essential for the homomeric interaction of SYD-2/Liprin-α protein in presynaptic assembly. *J. Neurosci.* 31:16261–16268. http://dx.doi.org/10.1523/JNEUROSCI.0002-11.2011

Toonen, R.F., K. Wierda, M.S. Sons, H. de Wit, L.N. Cornelisse, A. Brussaard, J.J. Plomp, and M. Verhage. 2006. Munc18-1 expression levels control synapse recovery by regulating readily releasable pool size. *Proc. Natl. Acad. Sci. USA*. 103:18332–18337. http://dx.doi.org/10.1073/pnas.0608507103

Tsuriel, S., A. Fisher, N. Wittenmayer, T. Dresbach, C.C. Garner, and N.E. Ziv. 2009. Exchange and redistribution dynamics of the cytoskeleton of the active zone molecule bassoon. *J. Neurosci.* 29:351–358. http://dx.doi.org/10.1523/JNEUROSCI.4777-08.2009

van Roessel, P., D.A. Elliott, I.M. Robinson, A. Prokop, and A.H. Brand. 2004. Independent regulation of synaptic size and activity by the anaphase-promoting complex. *Cell*. 119:707–718. http://dx.doi.org/10.1016/j.cell.2004.11.028

Weber, J.P., K. Reim, and J.B. Sørensen. 2010. Opposing functions of two sub-domains of the SNARE-complex in neurotransmission. *EMBO J.* 29:2477–2490. http://dx.doi.org/10.1038/emboj.2010.130

Wei, Z., S. Zheng, S.A. Spangler, C. Yu, C.C. Hoogenraad, and M. Zhang. 2011. Liprin-mediated large signaling complex organization revealed by the liprin-α/CASK and liprin-α/liprin-β complex structures. *Mol. Cell*. 43:586–598. http://dx.doi.org/10.1016/j.molcel.2011.07.021

Weston, M.C., R.B. Nehring, S.M. Wojcik, and C. Rosenmund. 2011. Interplay between VGLUT isoforms and endophilin A1 regulates neurotransmitter release and short-term plasticity. *Neuron*. 69:1147–1159. http://dx.doi.org/10.1016/j.neuron.2011.02.002

Wierda, K.D., R.F. Toonen, H. de Wit, A.B. Brussaard, and M. Verhage. 2007. Interdependence of PKC-dependent and PKC-independent pathways for presynaptic plasticity. *Neuron*. 54:275–290. http://dx.doi.org/10.1016/j.neuron.2007.04.001

Wyszynski, M., E. Kim, A.W. Dunah, M. Passafaro, J.G. Valtschanoff, C. Serra-Pagès, M. Streuli, R.J. Weinberg, and M. Sheng. 2002. Interaction between GRIP and liprin-alpha/SYD2 is required for AMPA receptor targeting. *Neuron*. 34:39–52. http://dx.doi.org/10.1016/S0896-6273(02)00640-2

Zhen, M., and Y. Jin. 1999. The liprin protein SYD-2 regulates the differentiation of presynaptic termini in *C. elegans*. *Nature*. 401:371–375.

Zürner, M., T. Mittelstaedt, S. tom Dieck, A. Becker, and S. Schoch. 2011. Analyses of the spatiotemporal expression and subcellular localization of liprin-α proteins. *J. Comp. Neurol.* 519:3019–3039. http://dx.doi.org/10.1002/cne.22664